Cranfield UNIVERSITY

The application of computational fluid dynamics to problems in rotorcraft aerodynamics: a literature review

Scott Shaw

COA Report No. 9502
April 1995

Department of Aerospace Science
College of Aeronautics
Cranfield University
Cranfield
Bedford MK43 0AL
England

Cranfield

College of Aeronautics Report No 9502
April 1995

The application of computational fluid dynamics to problems in rotorcraft aerodynamics: A literature review.

Scott Shaw

Department of Aerospace Science
College of Aeronautics
Cranfield University
Cranfield, Bedford MK43 0AL. England

ISBN 1871315557

£8

Abstract.

The flowfield around a helicopter rotor in forward flight is intrinsically unsteady and contains many complex interacting flow phenomena. As a consequence experimental investigations are difficult to perform, difficult to interpret and costly. There is a clear need for reliable computational methods whose uncertainties are less than those of experiment. In this paper computational methods currently available for the solution of problems in rotor aerodynamics are examined and the current direction of research in this field identified.

1. Introduction.

Methods for the calculation of the flowfield around helicopter rotor blades are much less well developed than those which are available to the fixed wing community. The major reason for this is the overall complexity of the flow physics which must be modelled which include varying freestream Mach number, varying incidence, dynamic stall and strong vortex interactions. At the present time the majority of codes which are in routine use for rotor aerodynamics are based upon the full potential equations, with coupling to wake analyses and boundary layer codes for lifting flows. Such codes contain considerable approximations to the flow physics and are incapable of predicting the flow behaviour on the retreating blade. In recent years work has been done to improve the physical modelling using the Euler and Navier-Stokes equations.

This paper begins with an introduction to the basic physical flow processes which any reliable (and complete) numerical method must seek to model if the rotor flowfield is to be calculated correctly. The solution of simplified forms of the basic equations of fluid dynamics is then considered in brief, followed by a more detailed analysis of solutions to the Navier-Stokes equations for rotor aerodynamics.

2. The flowfield of a helicopter in forward flight.

The flow about a helicopter rotor in forward flight is asymmetric and consequently the blades experience large variations in spanwise dynamic pressure, with a resultant large rolling moment about the rotor hub. This problem was overcome by de la Cierve who in 1923 introduced a flapping hinge in his autogyro design. The flapping hinge relieves the large hub rolling moment by allowing the rotor blades to flap, thus changing their local effective angle of incidence. The resulting flow is then one in which the advancing blade operates at high Mach number and low angle of incidence, while the retreating blade operates at high angle of incidence (often well above the static stall angle of incidence of the rotor aerofoil) and low Mach number. Other important flow features include the complicated helical wake and the strong tip vortices which are shed by the rotor blades and with which following blades may interact.

In this section the basic physical processes, see Figure 1 (from Caradonna[1]), which must be modelled if accurate predictions of the rotor flowfield are to be obtained, are described.

2.1 Compressibility effects.

The distribution of freestream Mach number in the azimuthal plane is described by Equation (2.1),

$$M_\infty = M_{tip} \{ \mu \sin(\psi) + r \} \qquad (2.1)$$

in which r is the non-dimensional spanwise location, ψ is the azimuth angle and μ is the advance ratio. At high advance ratios a region of transonic flow may develop (depending on the tip Mach number) over the outboard region of the advancing blade, this is shown in Figure (2) where contours of freestream Mach number are plotted

over the rotor disc for an advance ratio of 0.45 and tip Mach number of 0.6.

The occurrence of transonic flow at a given spanwise location is unsteady for rotors in forward flight with large variations in both shock strength and shock location occurring. For azimuthal angles between 0 and 90 degrees the flow is accelerating and the shock wave will increase in magnitude and move towards the rotor leading edge with increasing azimuth angle. The flow is decelerating for azimuth angles in the range 90 to 180 degrees where the shock wave will continue to move towards the leading edge while gradually reducing in strength. This is clearly demonstrated in Figure (3), taken from Reference (2), which shows the chordwise variation in local Mach number for three azimuthal angles, 60, 90 and 120 degrees. The unsteady nature of the flow is clearly evident from the symmetric azimuths (60 and 120 degrees) where the chordwise Mach number distributions would be expected to be identical in a steady flow or quasi-steady flow.

Where the shock is of sufficient strength to cause shock induced separation the flow will be strongly three-dimensional. The ability to calculate transonic flows in the rotor flowfield is of great practical importance as the onset of wave drag is a major limiting factor in the aerodynamic performance of the rotor blade. Additionally if the tip Mach number is highly supercritical then delocalisation may occur at the blade tip, the occurrence of this phenomena may represent a significant contribution to the overall level of noise which can be attributed to the rotor aerodynamics.

2.2 Blade vortex interaction (BVI).

A significant proportion of the overall lift generated by a helicopter rotor is developed over a very small extent of the span close to the tip. Such a concentration of aerodynamic loading leads to the formation of a very strong tip vortex which is shed into the wake. This tip vortex is persistent and may interact with following rotor

blades. For rotors which are in hover or vertical descent the tip vortex will impinge directly onto the following blades and strong blade vortex interactions of the type described in Reference (4) will occur. The importance of such interactions is clearly evident in Figure (4) (taken from Reference (4)) which shows bifurcation of a shock on the advancing blade as a direct result of the blade vortex interaction. In forward flight at high advance ratios blade vortex interaction is much less significant as the tip vortices are convected downstream of the rotor disc at the freestream velocity.

The ability to model blade vortex interactions correctly is important because this phenomena not only affects aerodynamic performance but also represents a major contribution to the overall noise of the helicopter.

2.3 Dynamic stall.

For a helicopter in forward flight the freestream velocity varies with azimuthal angle in the manner described by Equation (2.1). This will in turn lead to a variation in the aerodynamic moment which, as the blades are hinged, produces blade flapping. The resulting motion of the rotor blade can be expressed in the form,

$$I\frac{\partial^2\beta}{\partial t^2} + \kappa\frac{\partial\beta}{\partial t} + k\beta = M_f \qquad (2.2)$$

in which M_f is the aerodynamic moment (which varies as a function of azimuth angle (ψ), I, κ and k are the moment of inertia, damping constant and spring constant of the blade respectively, and β is the blade flapping angle. Equation (2.2) may be solved for β as a Fourier series of the form,

$$\beta(t) = \beta_o - \sum_{n=1}^{N} a_n \cos(n\psi) + b_n \sin(n\psi) \qquad (2.3)$$

In which β_o is the coning angle and the azimuth angle is a function of time

The effects of the flapping motion described by Equation (2.3) are to induce

angle of attack variations such that the retreating blade operates at a much higher incidence than the advancing blade. This angle of incidence is often well in excess of the static stall angle of attack of the rotor aerofoil due to the unsteady nature of the flow. Stall is delayed to a much higher angle of attack and is much more severe than that which would be experienced at the static stall angle of attack. This phenomena is known as dynamic stall. The sequence of events which occur after the static stall angle is passed are illustrated in Figure (5) (from Reference (5)) for the NACA 0012 aerofoil. As the aerofoil passes the static stall angle of attack reversed flow begins to develop in the boundary layer towards the trailing edge. With increasing incidence this region of reversed flow grows so that it extends over a much greater proportion of the chord and the boundary layer begins to thicken. Eventually the boundary layer will separate from the aerofoil surface and a strong vortical flow develops close to the leading edge which contributes significantly to the overall lift of the aerofoil. This region of vortical flow moves downstream with increasing incidence until it is shed into the wake at which time lift stall begins. The flow then remains stalled until the boundary layer becomes re-attached to the aerofoil surface, which is often not until after the incidence has returned to a value well below that of static stall. This behaviour results in a lift hysterisis loop of the type shown in Figure (5). Figures (6) and (7) show flow visualisations of aerofoils undergoing dynamic stall which have been obtained by experiment[6] and computation[7].

The dynamic stall of helicopter rotors is of great practical significance during high speed forward flight as its occurrence restricts the maximum forward flight speed, interestingly this is the opposite of the situation found for fixed wing aircraft where the angle at which stall occurs imposes a limit on the minimum forward flight speed.

2.4 Reversed flow.

In forward flight Equation (2.1) describes a region of the flow field in which the direction of flow is reversed. This region exists on the retreating blade for spanwise stations where,

$$\mu|\sin(\psi)| > r \tag{2.4}$$

The occurrence of reversed flow and incompressible flow near to the hub presents a major challenge to current computational methods based upon compressible formulations of the governing equations. At the present time incompressible flow solvers must be employed at low Mach numbers, below 0.1, if reliable results are to be obtained. Due to the small contribution of regions close to the hub to the overall aerodynamic forces it may be possible to neglect this region of the rotor blade without any significant reduction in the accuracy of the method used.

2.5 Rotor Wake.

The flowfield around helicopter rotors in hover is dominated by a complicated helical wake. This wake can generally be considered to be both incompressible and inviscid (although it is generated by viscous effects) as it is generally confined to thin layers away from the main rotor, which while convected by the global flow do not interact with it. The calculation of the geometry of the rotor wake remains one of the most difficult and most studied problems in helicopter rotor aerodynamics. The geometry of the rotor wake becomes very complicated in forward flight although it is a much less dominant feature of the flowfield as it is convected away from the rotor at the forward flight speed of the helicopter.

3. The calculation of the flowfield around helicopter rotors.

A large number of computational tools have been developed within the last 20 years to predict the flowfield around helicopter rotors. The solvers differ mainly in their choice for the governing equations (full potential, Euler or Navier-Stokes) and while less sophisticated models are unable to directly predict many of the flow features which have been described in Section 2 they are able to produce useful results using limited computational resources.

In the following sections solutions of the full potential, Euler and Navier-Stokes equations are considered in turn.

3.1 The solution of the Full potential equations.

Until very recently the most common flow analyses were those based upon the solution of the full potential equations. This class of flow solvers is by far the most efficient, although much of the underlying flow physics are lost in the assumptions which must be made. Considerable work has been done to extend the validity of the full potential equations by coupling the governing equations with additional theoretical and empirical models to allow the prediction of phenomena such as blade vortex interactions, retreating blade dynamic stall and the rotor wake. A detailed review of this work is beyond the scope of the present report and so only a brief description is presented here. The interested reader is directed to the excellent reviews of this field by Carradonna[1,8,9].

The full Navier-Stokes equations, which are thought to describe the dynamics of a fluid exactly, may be considerably simplified by assuming that the flow is both inviscid and irrotational. The resulting velocity vector field **U** can then be described by the gradient of a potential function, Φ.

$$\text{i.e.} \qquad \mathbf{U} = \nabla\Phi \tag{3.1}$$

This represents a considerable simplification of the problem which must then be solved because not only are the three velocity components (u, v, w) now replaced by a single variable, but also the four differential equations which describe the conservation of momentum (three equations) and conservation of energy, are now replaced by a single algebraic expression, Bernoulli's equation,

$$\frac{\rho}{\rho_\infty} = \left[1 - \frac{\gamma - 1}{a^2}\left(\Phi_t + \frac{1}{2}(\nabla\Phi)^2\right)\right] \tag{3.2}$$

Taking Equation (3.2) together with the continuity equation,

$$\frac{\partial \rho}{\partial t} + \nabla\rho\Phi = 0 \tag{3.3}$$

a closed system of equations is obtained for non-lifting bodies. In order to close the system of equations for lifting bodies it is necessary to specify a jump condition at the trailing edge which ensures that the potential remains single valued, this is the well known Kutta condition.

This system of equations, known as the full potential equations, requires significantly less computation, running at least five times faster than a comparable Euler solver [10]. The assumptions which have been made do however represent a considerable simplification of the flow physics which are involved, and the method must be extended by coupling with further analytical and empirical expressions if the flow features described in Section 2 are to be modelled.

If the flow is considered to be inviscid then dynamic stall of the retreating blade cannot be addressed. The potential flow equations may be extended to include viscous effects by coupling with an appropriate boundary layer model [11]. It may then be possible to obtain reasonable agreement with experimental data for cases in which the flow is lightly stalled [12], see Figure (9). Massively separated flows, which are of

much greater importance in the study of dynamic stall, remain beyond the scope of this method.

The rotor wake can be considered to be inviscid (and incompressible) as it is generally confined to thin layers which while convected by the global flow, do not interact with it. While the assumption that the wake is inviscid is valid, without the inclusion of viscous terms in the governing equations there is no mechanism by which it can be generated. If the influence of the wake is to be accounted for then it must be modelled directly, modelling of the wake geometry can be addressed in one of two ways, either by specifying the wake geometry fully at the beginning of the calculation, the prescribed wake approach, or by extending the governing equations using additional terms, usually this is achieved by coupling the flow analysis code with an independent wake analysis method, in order to improve the modelling of the physics involved, this is the free wake approach (a parallel can be drawn here with the shock fitting and shock capturing techniques commonly employed for the calculation of transonic flows).

In the fixed wake approach the structure of the wake is related to the calculated thrust coefficient and blade geometry empirically by means of an experimental database. This approach is very restrictive, limiting the blade geometry which may be considered to those which are similar to the geometry's contained within the database. For any unconventional blade geometry, such as that of the BERP rotor[13] which has a novel planform close to the tip, a new empirical relationship must first be developed before reliable calculations can be expected. The freewake method is much less restrictive in this respect and is applicable to a much wider range of configurations. In the freewake approach the model is extended to include additional terms and equations which describe the evolution of the rotor wake geometry over

time. An initial guess may then be made and the wake geometry found by iterating between the potential flow solver and the wake geometry equations. Despite the improved physical modelling which this approach offers it has been found by a number of authors that this method provides solutions which are no more accurate than those obtained with a prescribed wake [14].

The simplification of the governing equations which follows from the assumption of irrotational flow has important consequences for the modelling of shock waves as momentum is no longer explicitly conserved (although mass is). It has been found over many years of use of the full potential equations that momentum is conserved provided that the flow is smooth (i.e. shock free). For flows which contain weak shock waves there is a non-physical pressure loss across the shock which correlates well with the Rankine-Hugoniot relationships. This correlation breaks down for shock waves of any significant strength and consequently the full potential equations must be extended if transonic flow is to be modelled. The governing equations may be extended by the introduction of either a non-isentropic density relationship[1] or a quasi-conservative factor[15]. In the first of these two approaches the density of points on, and close to, the shock is expressed by,

$$\rho = \rho_{isen}\, e^{ds/R} \tag{3.4}$$

where ds is the shock generated entropy determined from the Rankine-Hugoniot relations. This approach is strictly only valid for steady flows but has been found to work reasonably well for unsteady flows also.

In the second approach Lock noted that the Rankine-Hugoniot shock jump relations suggested that the strength of the physical shock wave lies somewhere between the strength determined by conservative (isentropic shock) and non-conservative (where the shock is only of sufficient strength to reduce the local Mach

number to just below one) potential flow schemes. Lock suggested a modified potential scheme in which,

$$\Phi = (1-\sigma)\,\Phi_{con} + \sigma\,\Phi_{non} \tag{3.5}$$

where Φ_{con} and Φ_{non} are the potentials determined by conservative and non-conservative schemes respectively and σ is the quasi-conservative factor which is problem dependent and determined by experimentation. The ability of the full potential methods to capture shock waves is demonstrated by the comparison with experiment shown in Figure (10).

Vorticity cannot exist in a potential flow field, except as discrete embedded elements (usually filaments or sheets) because in deriving the governing equations the flow has been assumed to be irrotational. As a consequence flow features which arise as a direct result of distributed vorticity, such as the tip vortices described in Section 2, cannot be captured at all. While such phenomena can be modelled using discrete vortical elements additional simplifications are required to describe their convection by the freestream as vorticity is not transported in the full potential equations.

Despite the many weaknesses of the full potential equations they have been shown to be able to provide reasonably accurate predictions (at low cost) of the helicopter rotor flow field when it can be considered to be essentially inviscid. In practice this means that the potential flow equations can be considered to provide a reliable model for all of the phenomena described in Section 2, except that of dynamic stall on the retreating blade.

3.2 Solutions of the Euler Equations.

During the past decade potential flow approximations for the unsteady transonic flow past helicopter rotor blades have matured to a point where there is very little scope for further significant improvements. Over the same period of time there has been a rapid increase in the availability of high powered computers which has allowed researchers in this field to focus their attention on more complete, but computationally more expensive, approximations to the flow field. In this section the solution of the Euler equations for rotor flow problems is considered.

The Euler equations describe the conservation of mass, momentum and energy in an inviscid, rotational fluid and are generally written, in a Cartesian frame of reference, in the form,

$$\frac{\partial Q}{\partial t} + \frac{\partial E}{\partial x} + \frac{\partial F}{\partial y} + \frac{\partial G}{\partial z} = 0 \tag{3.6}$$

where Q is the vector of conservative variables and E, F and G are the flux vectors obtained from,

$$Q = \begin{pmatrix} \rho \\ \rho u \\ \rho v \\ \rho w \\ E_t \end{pmatrix} \quad E = \begin{pmatrix} \rho u \\ \rho u^2 + P \\ \rho uv \\ puw \\ u(E_t + P) \end{pmatrix} \quad F = \begin{pmatrix} \rho v \\ \rho uv \\ \rho v^2 + P \\ \rho vw \\ v(E_t + P) \end{pmatrix} \quad G = \begin{pmatrix} \rho w \\ \rho uw \\ \rho vw \\ \rho w^2 + P \\ w(E_t + P) \end{pmatrix}$$

Here ρ is the density, u,v and w are the components of velocity in the x,y and z directions respectively, P is the pressure and E_t is the total energy per unit volume.

In principal this system of equations can accurately describe the creation and convection of vorticity (although only vorticity due to inviscid flow phenomena, such as shock waves, can be created). Unlike the full potential equations, where the simplification of the governing equations following the assumption of irrotational

flow allows a relaxation of the condition that momentum be conserved, the Euler equations explicitly conserve both mass and momentum. As a consequence the Rankine-Hugoniot relations across flow discontinuities are satisfied for strong shock waves.

Equation (3.6) is in a form which is unsuitable for the solution of flow problems around bodies of arbitrary shape and is therefore more usually written in a body fitted co-ordinate scheme as,

$$\frac{\partial Q}{\partial t}+\frac{\partial \overline{E}}{\partial \varepsilon}+\frac{\partial \overline{F}}{\partial \eta}+\frac{\partial \overline{G}}{\partial \zeta}=0 \qquad (3.7)$$

in which $Q = J^{-1}Q$, $\overline{E} = J^{-1}\left(E\frac{\partial \varepsilon}{\partial x}+F\frac{\partial \varepsilon}{\partial y}+G\frac{\partial \varepsilon}{\partial z}\right)$ etc.

Here J is the Jacobian and $\partial\varepsilon/\partial x$, $\partial\varepsilon/\partial y$, $\partial\varepsilon/\partial z$ etc. are the metrics of the transformation.

In order to solve the above equations boundary conditions must be specified along the rotor surface and the far field boundaries. Along the rotor surface the velocity components u, v and w are specified by the requirement that the surface normal velocity be zero, as there can be no transfer of mass or momentum across solid surfaces. The Euler equations therefore only require that the surface pressure distribution be known and this is normally obtained by assuming that the normal pressure gradient across the boundary layer at the wall be zero,

$$\text{i.e.} \quad \frac{\partial P}{\partial \eta} = 0 \qquad (3.8)$$

This assumption represents the neglecting of the centrifugal terms in the normal momentum equation which is not thought to cause calculations to be in significant error[10]. Deese and Argarwal[16,17] use an alternative method of calculating the surface pressure distribution in which the rate of change of normal momentum at

the wall with time is assumed to be zero,

$$\text{i.e.} \qquad \frac{\partial(\rho V_n)}{\partial t} = 0 \tag{3.9}$$

where V_n is the wall normal velocity. The pressure gradient at the wall is then determined using the normal momentum equation which should then allow a much better approximation to the wall pressure distribution to be obtained. Special care must be taken in applying these boundary conditions at the blade root where infinite sweep assumptions are invoked. Under these assumptions spanwise gradients are considered to be negligible and consequently the flux vector in the spanwise direction may be dropped from the governing equations.

Boundary conditions are determined for the outer boundaries by consideration of the direction of the flow at each outer boundary grid point. At both subsonic and supersonic inflow boundaries the required primitive variables (usually pressure, density and the three velocity components) are assigned their respective freestream values. At subsonic outflow boundaries the pressure is normally specified and the remaining data is extrapolated from the interior while at supersonic outflow boundaries all of the required primitive variables are determined by extrapolation from the interior of the computational domain.

The boundary conditions listed above are sufficient for the calculation of the flowfield around non-lifting rotors in both hover and forward flight. For lifting rotors these boundary conditions must be altered to fully account for the effects of the boundary layer, wake and tip vortices. As the Euler equations do not include any viscous terms explicitly they are unable to model any of these flow features directly. These phenomena are most commonly modelled by coupling the flow analysis code

with additional boundary layer and wake models.

Boundary layer effects are normally modelled by relaxing the condition that the wall normal velocity be zero and introducing a specified non-zero wall normal velocity distribution (the so called transpiration velocity) which is determined from a suitable boundary layer analysis, this approach is considered in detail by Lock and Williams.[11]

The inclusion of the influence of shed vorticity (the wake and the tip vortices) is complicated by the fact that the computational domain is constructed around a single blade which only captures the near wake, see Figure (11). The remainder of the wake and the tip vortices shed by preceding blades are not seen by the computational grid and must be modelled using a wake analysis code, such as those used in the solution of the potential flow equations. Such analyses are based on incompressible lifting line theory with a linear distribution of vorticity along the span, except close to the tip. The wake is assumed to be a helical spiral which is modelled by a distribution of point vorticity and is free to contract and expand in response to the local self induced velocity. The Biot-Savat law is then applied to this system of vortical elements which results to determine the local downwash angle which can then be used to specify a distribution of non-zero transpiration velocity along the blade span. Coupling of the governing equations with such models allow the extension of the Euler equations to the calculation of the flowfield around lifting rotors, however it is readily apparent that such models do not represent a significant step forward from the full potential equations.

The ability of the Euler equations to accurately model the creation and convection of vorticity represents an important step forward from the full potential equations in the approximation of the flowfield about helicopter rotors which may be

dominated by a vortical wake and blade vortex interactions. Unfortunately the Euler equations are most often solved using finite difference approaches which will unavoidably introduce false dissipation of vorticity leading to significant errors in the flowfield calculation .

In the finite difference approach approximations to derivatives are obtained by a Taylor series expansion of the form,

$$f(x+\Delta x) = f(x) + \Delta x \frac{\partial f}{\partial x}(x) + O(\Delta x^2) \qquad (3.10)$$

where $O(\Delta x^2)$ is the truncation error and is of order Δx^2. Rearranging gives,

$$\Delta x \frac{\partial f}{\partial x}(x) = f(x+h) - f(x) - O(\Delta x^2) \qquad (3.11)$$

The truncation error can be regarded as a non-physical viscosity which will act to dissipate vorticity. The problem of numerical dissipation was studied by Rai[4] who examined the convection of a Lamb type vortex in an inviscid freestream using a Beam-Warming implicit scheme of variable temporal and spatial order. Rai's conclusions are summarised in Figure (12) which clearly shows the importance of higher order schemes and finer grids in reducing false dissipation, of particular note is curve A which demonstrates very clearly that first order schemes in time are unsuitable for studying problems in which the convection of vorticity is of importance.

While a higher order scheme, fifth order and above, is desirable for maintaining accuracy schemes of this order are generally impractical as the increased stencil which results requires a much greater number of arithmetic operations per grid point increasing CPU time significantly.

The use of central differences to approximate derivatives will usually require the introduction of an arbitrary smoothing parameter, usually referred to as artificial

viscosity, to smooth spurious oscillations in the numerical solution which occur near strong discontinuities, such as shock waves. The added terms correspond to second and fourth order derivatives and have a similar form to the viscous terms in the complete Navier-Stokes equation. This non-physical viscosity may cause a rapid dissipation of vorticity and consequently degrade or prevent accurate modelling of vortical phenomena. The need to add artificial viscosity in this way is avoided by the use of upwind finite difference schemes, some care is required in selecting such a scheme as the numerical dissipation due to the truncation error is often much higher than that found in a central difference scheme.[4]

In addition to the truncation error and explicitly added artificial viscosity there are also contributions to the numerical dissipation of a computational method, although of much lesser significance, from the accuracy of surface and farfield boundary conditions, smoothness of the grid and the rounding error of the computer on which the calculations are performed.

Sankar and Tung[10] have solved the Euler equations in a body fitted moving co-ordinate system using an approximately factored implicit solver with explicitly added second and fourth order artificial viscosity. The Euler solver was coupled with an incompressible free wake analysis code (CAMRAD) for the calculation of the flowfield around lifting rotors. Agreement with experiment was found to be excellent for non-lifting rotors and reasonably good for lifting rotors, see Figure (16), the apparent over prediction of the leading edge suction peak is an artefact of the use of a trim analysis code, which while accurately matching the specified thrust coefficient does not necessarily match the collective and cyclic pitch angles which were measured in the experiment. The position of the shock wave appears to have been captured accurately, although the shock strength is over predicted because the effect of

the boundary layer (which acts to reduce shock strength) has not been included in the model.

The use of compact operator schemes to extend the order of the finite difference approximation has been examined by Smith and Sankar[18] who modified an existing second order in space, Euler method for the transonic, steady flow of rotors in hover. In their modified scheme streamwise and normal derivatives are evaluated by weighting the derivative of a point i,j,k with the derivatives of points on either side, using the streamwise derivative of E as an example,

$$E_\varepsilon = \alpha(E_{i-1})_\varepsilon + (E_i)_\varepsilon + \alpha(E_{i+1})_\varepsilon = \frac{a}{2\Delta\varepsilon}(E_{i+1,j,k} - E_{i-1,j,k}) + \frac{b}{4\Delta\varepsilon}(E_{i+2,j,k} - E_{i-2,j,k}) \tag{3.12}$$

in which $\Delta\varepsilon$ is the cell size in the streamwise direction and,

$$a = 2/3\ (\alpha + 2) \quad \text{and} \quad b = 1/2\ (4\alpha - 1)$$

The order of the scheme is determined by the coefficient α, for $\alpha = 0$ and $\alpha = 1/3$ fourth and sixth order operators are obtained. In Reference (18) α=1/4 was employed to provide a fourth order operator with a compact stencil (as b=0 in this case). This procedure leads to a system of 5 scalar tri-diagonal matrices for each of the fluxes at every point in the flow domain which can be solved to obtain the required fluxes using the Thomas algorithm. Smith and Sankar report an increase in CPU time of around 1.5% per grid point based upon a comparison with the original scheme.

The significance of the use of compact operators to obtain higher order approximations to the fluxes lies in the subsequent reduction in the number of grid points which are required which arises as a consequence of the increased order of the scheme. In Figure (13) results are presented which suggest that it is possible to achieve a 50% reduction in the number of streamwise grid points while maintaining

the same level of accuracy as the original second order scheme (this represents an approximate halving of the total computational time which is required).

The compressible Euler equations have been solved by Deese and Argarwal[16,17] and Tung and Chang[19,20] using a finite volume approach in a blade fixed Cartesian frame of reference rotating with the angular velocity, Ω, of the rotor. The governing equations are rewritten in the form,

$$\frac{\partial Q}{\partial t}+\frac{\partial E}{\partial x}+\frac{\partial F}{\partial y}+\frac{\partial G}{\partial z}+u_{\Omega}\frac{\partial Q}{\partial x}+w_{\Omega}\frac{\partial Q}{\partial x}=C \qquad (3.13)$$

where u_{Ω} and w_{Ω} are the rotational velocity components and C is given as,

$$C=\begin{pmatrix}0\\-\rho\Omega w\\0\\\rho\Omega u\\0\end{pmatrix}$$

This formulation of the Euler equations allows a much more accurate calculation of flux terms as the flow at in the far field is uniform, although the relative flow is not. The additional accuracy which the solution of this set of governing equations offers is essential if an accurate solution is to be obtained using the finite volume approach which was adopted[16]. Calculation for lifting rotors were carried out using a wake analysis technique which produced local changes to the effective angle of attack. Excellent agreement was obtained between calculation and experimental measurements for a non-lifting rotor in hover, part (a) of Figure (14). For lifting rotors the agreement remains good, both in hover and for forward flight (parts (b) and (c) of Figure (14) respectively.). Perhaps of more significance is the disappointing comparison of results obtained from an Euler code and full potential code, Figure (15), which seems to indicate that there is no significant overall improvement in

accuracy, although the shock does appear to have been captured more sharply, when using the Euler equations.

Methods for the calculation of rotor flows using the Euler equations are much less well developed than those methods which use the full potential equation. Results from currently available codes indicate that it is possible to achieve excellent comparison between experiment and calculations for non-lifting rotors and good comparison for lifting rotors. The comparison of the accuracy of current Euler codes with state of the art full potential solvers is disappointing and seems to suggest that no significant improvements have been achieved by using the computationally more expensive Euler methods. The calculation of lifting flows is currently achieved by coupling of the Euler solver with a freewake analysis method. In all of the methods which were examined the effects of the boundary layer were neglected with a consequent over prediction of shock strength, the inclusion of viscous effects (perhaps by coupling with a suitable boundary layer analysis code) would seem to be a desirable short term objective for increasing the overall accuracy of such methods.

The use of higher order approximations for the flux terms has produced some encouraging results for studies involving blade vortex interaction, however the inability of the Euler equations to model correctly the creation of vorticity at the blade tips remains a major drawback for such studies.

3.3 Solutions of the Navier-Stokes equations.

Numerical schemes based upon inviscid governing equations, such as the Euler equations and full potential methods described in the previos two sections, are able to reliably predict attached compressible flow around helicopter rotors in both hover and forward flight. The flow around the retreating rotor blade, and also the tip of the advancing blade, is dominated by viscous phenomena and consequently the inviscid assumption is no longer valid. In order to include the effects of viscosity the full Navier-Stokes equations must be solved. The full Navier-Stokes equations are significantly more expensive to solve than the Euler equations because of the requirement for high grid density in order to resolve the boundary layer accurately, this has meant that that significant progress in solving the unsteady compressible Navier-Stokes equations for helicopter rotors has only become practical very recently with the advent of high powered workstations and more widely available super computing facilities.

The Navier-Stokes equations may be written for a body fitted curvilinear co-ordinate system in the form,

$$\frac{\partial Q}{\partial t}+\frac{\partial(E-E_v)}{\partial \varepsilon}+\frac{\partial(F-F_v)}{\partial \eta}+\frac{\partial(G-G_v)}{\partial \zeta}=0 \qquad (3.14)$$

in which Q is the vector of the conservative variables E, F, and G are the inviscid flux vectors and E_v, F_v and G_v are the viscous flux vectors. The inviscid flux vectors are given by,

$$Q=\begin{pmatrix}\rho\\ \rho u\\ \rho v\\ \rho w\\ E_t\end{pmatrix},\quad E=\begin{pmatrix}\rho U\\ \rho uU+\varepsilon_x P\\ \rho vU+\varepsilon_y P\\ \rho wU+\varepsilon_z P\\ (E_t+P)U+\varepsilon_t P\end{pmatrix}, \qquad (3.15(a))$$

$$F=\begin{pmatrix}\rho V\\ \rho uV+\eta_x P\\ \rho vV+\eta_y P\\ \rho wV+\eta_z P\\ (E_t+P)V+\eta_t P\end{pmatrix},G=\begin{pmatrix}\rho W\\ \rho uW+\zeta_x P\\ \rho vW+\zeta_y P\\ \rho wW+\zeta_z P\\ (E_t+P)W+\zeta_t P\end{pmatrix} \qquad (3.15(b))$$

here E_t is the total energy per unit volume, P is the pressure which may be obtained from the equation of state, J is the Jacobian of the transformation and ε_x, ε_y, ε_z, η_x, η_y, η_z, ζ_x, ζ_y and ζ_z are the metrics of the transformation. U, V and W are the contravariant velocities defined by,

$$\begin{aligned}U&=\varepsilon_x(u-x_t)+\varepsilon_y(v-y_t)+\varepsilon_z(w-z_t)\\ V&=\eta_x(u-x_t)+\eta_y(v-y_t)+\eta_z(w-z_t)\\ w&=\zeta_x(u-x_t)+\zeta_y(v-y_t)+\zeta_z(w-z_t)\end{aligned} \qquad (3.16)$$

The grid velocity terms , x_t, y_t and z_t, contained in Equation (3.16) represent the motion of the grid relative to the inertial co-ordinate system (x,y,z). The viscous flux vectors are obtained from,

$$E_v=J^{-1}\begin{bmatrix}0\\ \varepsilon_x\tau_{xx}+\varepsilon_y\tau_{xy}+\varepsilon_z\tau_{xz}\\ \varepsilon_x\tau_{xy}+\varepsilon_y\tau_{yy}+\varepsilon_z\tau_{yz}\\ \varepsilon_x\tau_{xz}+\varepsilon_y\tau_{yz}+\varepsilon_z\tau_{zz}\\ \varepsilon_x\beta_x+\varepsilon_y\beta_y+\varepsilon_z\beta_z\end{bmatrix},\quad F_v=J^{-1}\begin{bmatrix}0\\ \eta_x\tau_{xx}+\eta_y\tau_{xy}+\eta_z\tau_{xz}\\ \eta_x\tau_{xy}+\eta_y\tau_{yy}+\eta_z\tau_{yz}\\ \eta_x\tau_{xz}+\eta_y\tau_{yz}+\eta_z\tau_{zz}\\ \eta_x\beta_x+\eta_y\beta_y+\eta_z\beta_z\end{bmatrix},$$

$$G_v=J^{-1}\begin{bmatrix}0\\ \zeta_x\tau_{xx}+\zeta_y\tau_{xy}+\zeta_z\tau_{xz}\\ \zeta_x\tau_{xy}+\zeta_y\tau_{yy}+\zeta_z\tau_{yz}\\ \zeta_x\tau_{xz}+\zeta_y\tau_{yz}+\zeta_z\tau_{zz}\\ \zeta_x\beta_x+\zeta_y\beta_y+\zeta_z\beta_z\end{bmatrix}. \qquad (3.17)$$

in which the shear stresses are defined as,

$$\tau_{xx}=\lambda(u_x+v_y+w_z)+2(\mu+\mu_T)u_x$$

$$\tau_{xy}=\tau_{yx}=(\mu+\mu_T)\,(u_y+v_x)$$

$$\tau_{xz}=\tau_{zx}=\lambda(\mu+\mu_T)\,(u_z+w_x)$$

$$\tau_{yy} = \lambda(u_x + v_y + w_z) + 2(\mu + \mu_T)v_y$$

$$\tau_{zz} = \lambda(u_x + v_y + w_z) + 2(\mu + \mu_T)w_z$$

$$\beta_x = \gamma\varepsilon_x(\mu/Pr + \mu_T/Pr_T) + u\tau_{xx} + v\tau_{xy} + w\tau_{xz} \qquad (3.18)$$

$$\beta_y = \gamma\varepsilon_y(\mu/Pr + \mu_T/Pr_T) + u\tau_{xy} + v\tau_{yy} + w\tau_{yz}$$

$$\beta_z = \gamma\varepsilon_z(\mu/Pr + \mu_T/Pr_T) + u\tau_{xz} + v\tau_{yz} + w\tau_{zz}$$

$$\varepsilon = E_t/\rho - (u^2 + v^2 + w^2)/2$$

where Pr is the Prandtl number (0.72 for air), λ is the bulk viscosity (obtained from Stokes theorem), Pr_T is the turbulent Prandtl number and μ_T is the turbulent viscosity.

This system of equations is incomplete for turbulent flows for which a turbulence model must be employed to calculate the turbulent eddy viscosity. The choice of turbulence model is critical to the success of calculations involving retreating blade dynamic stall and is considered in some detail later in this section.

In addition to the above equations boundary conditions must also be specified along the rotor blade surface and at the farfield boundaries. At the surface of the rotor blade no-slip conditions are applied, that is the three components of velocity are all set equal to zero. In addition to the conditions imposed upon the velocity at the rotor blade surface two other parameters must be specified (usually pressure and temperature) and are usually obtained by setting their respective normal derivatives to zero at the blade surface.

At the innermost point of the rotor blade the spanwise flux is usually taken to be zero, i.e. the flow is considered to be quasi two-dimensional. Provided that the rotor blade is of high aspect ratio and the hub is sufficiently far from the rotor tip the application of the infinite sweep assumption in this manner is a suitable approximation.

Boundary conditions are specified at the outer boundaries by consideration of the characteristic solutions. For boundaries at which the flow is subsonic extrapolated and freestream Riemann invariants (which are constant along characteristic lines) of the form,

$$R = V_n - \frac{2a}{\gamma - 1} \tag{3.19}$$

are used to obtain the normal velocity and local speed of sound using the following relationships,

$$\begin{aligned} V_n &= \frac{1}{2}(R_e - R_\infty) \\ a &= \frac{\gamma - 1}{4}(R_e - R_\infty) \end{aligned} \tag{3.20}$$

where R_∞ is the freestream Riemann invariant and R_e is the Riemann invariant extrapolated from the computational domain. At an inflow boundary the tangential velocity and entropy are also specified (using the freestream values) while at an outflow boundary tangential velocity and entropy are determined by extrapolation from within the computational domain.

For supersonic flows the required primitive variables are either all specified (inflow boundaries) or extrapolated from the interior of the domain (outflow boundaries).

Like the Euler equations the above boundary conditions are insufficient for the calculation of lifting rotors. For lifting flows the influence of the portion of the wake which lies outside of the computational domain and tip vortices from proceeding blades must all be accounted for. The influence of the shed vorticity is included using a wake analysis method similar to those employed in the solution of both the full potential and the Euler equations. The wake analysis method is used to calculate the

upwash along the rotor surface due to the wake, this information is then added to the Navier-Stokes solution by specifying a non-zero transpiration (i.e. normal to the surface) velocity distribution.

As with the Euler equations the flux terms in the Navier-Stokes equations are normally approximated using finite differences and consequently suffer similar problems with false dissipation of vorticity. The use of higher order approximations for the flux terms, described in the previous section, to reduce the magnitude of the numerical dissipation has been tried with some success by Smith and Sankar[18] for rotors in hover and by Rai[4] for blade vortex interactions. The use of higher order spatial approximations with the Navier-Stokes equations has also been investigated by Ekaterinaris[21] who studied the flowfield around delta wings at high angle of attacks where the aerodynamics are dominated by strong vortical structures. In this work the flowfield was divided into two discrete regions, a viscous inner region (where the Navier-Stokes equations were applied) and an outer inviscid region (where the Euler equations were used). Ekaterinaris was able to show that the use of higher order approximations for the flux terms was only required in the outer inviscid region where the grid density was much lower than in the viscous inner region. This work would seem to suggest that higher order approximations need only be used for the inviscid flux terms even when the flowfield is considered as a single entity.

False dissipation of vorticity as a consequence of added artificial viscosity should be much reduced in the solution of the Navier-Stokes equation as the presence of physical viscosity reduces the level of artificial viscosity which is required to control spurious oscillations in the solution, much greater care is required in the application of this artificial viscosity to ensure that it does not lead to inaccuracies in the region of the boundary layer.

The solution of the unsteady Navier-Stokes equations for the flowfield around helicopter rotor blades offers the opportunity to study the dynamic stall of the retreating blade. The flowfield around wings and bodies undergoing oscillatory motions is usually turbulent and some consideration must therefore be given to the choice of an appropriate turbulence model for use with the Navier-Stokes equations. At high oscillatory frequencies the flowfield is dominated by the forcing motion, because the characteristic time scale of the forcing motion is much smaller than that of the turbulence, and so discrepancies between calculations where the flow is considered fully laminar and experimental measurements are relatively small. As the oscillatory frequency is reduced the influence of turbulence becomes more important. The rotational frequency of helicopter rotor blades is relatively small, typically between 5 and 10 revolutions per second, and consequently special care must be taken in choosing an appropriate turbulence model.

There are a large number of turbulence models available in the literature ranging from simple algebraic models, such as that due to Baldwin and Lomax, to models which require the solution of a number of ordinary differential equations, such as the k-ε model. The selection of a turbulence model will to some extent be a compromise between accuracy and computational cost. The relative computational costs of several popular turbulence models (Baldwin-Lomax (BL), Renormalization group theory (RNG), Baldwin-Barth (BB), Johnson-King (JK) and Spalart-Allmaras (SA)) are compared in Figure (17).

The most widely used turbulence model is the Baldwin-Lomax algebraic turbulence model. This model is simple to implement and relatively inexpensive, it has been shown to produce very good agreement with experimental measurements for steady attached flows and flows in which there is only a mild separation. For steady

accurately and consistently model the flow physics involved in dynamic stall. Additionally the results of Ekaterinaris and Menter suggest that consideration of transitional modelling must be made, even at high Reynolds numbers. The modelling of transition is likely to be of increased importance for the range of Reynolds numbers over which helicopter rotor blades currently operate.

Solutions of the steady compressible Navier-Stokes equations for fixed wings have been available in the literature for some time and have been used by researchers in the field of helicopter aerodynamics to provide additional qualitative insight into some of the physical phenomena encountered in the flowfield of a rotor blade. Most recently Scott and Narramore[26] have studied the formation of tip vortices with a steady Navier-Stokes solver and achieved very good agreement with experiment.

The first published solutions of the Navier-Stokes equations for the unsteady, compressible three-dimensional flow around helicopter rotors were presented by Wake[27] and Wake and Sankar[28] for non-lifting rotors in hover and forward flight and lifting rotors in forward flight. Their solver, which was based upon a code originally developed for the solution of the Euler equations, utilised a mixed implicit/explicit ADI based approach which was only first order accurate (and also non-conservative) in time. Calculated results for non-lifting rotors in hover and forward flight were found to give much closer agreement with experiment than had previously been obtained using an Euler based approach, Figure (23). Comparison between calculation and experiment was also found to be good over the majority of the span for a lifting rotor, although poor grid resolution led to inaccurate results close to the tip.

The unsteady thin layer Navier-Stokes equations were solved by Srinivasan and McCroskey[29] in a frame of reference fixed to and rotating with the rotor blade using a fully implicit approximately factored ADI approach. Good agreement was

found between the calculated results and experimental measurements for non-lifting rotor blades in hover. Comparison was also made with the experimental results of Caradonna and Tung[30] for a lifting rotor in hover. A crude wake model was employed in which a constant angle of attack correction was made for the wake, the downwash angle was set equal to -3.8 degrees (this value having been obtained in previous Euler calculations). Comparison with experimentally determined pressure distributions at selected azimuth positions was found to be generally good for calculations in which the flowfield is wholly subsonic and fair under transonic flow conditions. Calculated values were found to compare poorly with measured values for spanwise stations close to the hub ($r/R < 0.5$) due to the poor wake modelling.

Srinivasan and McCroskey also examined the solution of the thin layer Navier-Stokes equations for the steady flow around fixed rotor blades with a variable distribution of spanwise freestream velocity. Calculations performed in this manner show a surprisingly good agreement with calculations carried out for the rotating rotor blade in hover, Figure (24) and flow visualisations of the calculated flowfield have shown that all of the primary features of the flowfield have been captured, More work is required to determine if secondary features of the flowfield are captured accurately but this work offers the opportunity for a much less computationally expensive method of calculating the flowfield around rotors in hover using existing steady solvers with minor modification to the freestream conditions.

Srinivasan and Baeder[30] have solved the thin layer Navier-Stokes equations in a blade fixed frame of reference using a fully implicit ADI approach with Roe's upwinding in all three spatial directions. For viscous flows an algebraic Baldwin-Lomax turbulence model was used to estimate the turbulent eddy viscosity. This method has been used with some success to calculate both lifting and non-lifting

flows around helicopter rotor blades in hover.

Srinivasan and Baeder extended their solution procedure to non-lifting rotor blades in forward flight in Reference (3) by solving the governing equations in an inertial frame of reference. Blade vortex interaction studies were also performed with encouraging results. Good qualitative and quantitative agreement was obtain with experimentally determined pressure fields, Figure (25), for vortices passing parallel and at oblique angles to the rotor blade. Measurements of acoustical data were also compared with the results of the computer code and showed that a good qualitative understanding of the acoustical details of the flowfield could be obtained from current Navier-Stokes solvers.

In Reference (31) Duque et al have examined the flow around BERP and UH-60A rotor blades in hover using the solution methodology of Srinivasan and Baeder[30,3] . Calculations were carried out without the use of a freewake analysis method and instead the influence of the wake was included in the specification of the farfield boundary conditions. For a computational domain of sufficient size the relative farfield velocities are all zero, unfortunately it is not practical for such a large domain to be used in current calculation procedures and so instead a non-zero distribution of velocity is specified along the outer boundaries. This distribution of velocity is determined from a consideration of mass flow conservation, the thrust produced by the rotor and simple one-dimensional momentum theories, a schematic of the new boundary conditions is shown in Figure (26).

Rajagopalan and Mather[14] have solved the incompressible, laminar, Navier-Stokes equations for forward flight using a finite volume based method known as SIMPLER. This method requires only blade geometry and aerofoil characteristic data

to obtain the full three-dimensional flowfield. Comparison with experiment ranges from poor to fair depending upon the flow conditions (advance ratio, freestream Mach number etc.). While this method is likely to be of little interest for the calculation of flows around single rotors (where much more reliable methods are available) its relative simplicity may allow the solution of much more complicated problems (such as the interference effects for main rotor/tail rotor or tandem rotor geometry's) with engineering accuracy. Such complicated flowfields are currently beyond traditional three-dimensional Navier-Stokes solvers.

Perhaps the most significant drawback associated with solutions of the full Navier-Stokes equations is their high computational cost. A method of reducing the computational demands for viscous solvers was investigated by Berezin and Sankar[32] who solved the Navier-Stokes equations near the blade and in the wake where viscous effects are important (inner region) and the full potential equations elsewhere (outer region). The two regions share a common interface along which the solvers are coupled, see Figure (27). Comparison with calculations performed using the Navier-Stokes solver as a stand alone method have shown that the new coupled method is in excellent agreement along the rotor blade surface, Figure (28), although in the flowfield there are some minor discrepancies, Figure (29). This work has shown that results of comparable quality with a stand alone Navier-Stokes method can be achieved in half of the computational time using a coupled approach.

At the present time no work has been published in which the Navier-Stokes equations are solved for the retreating side of the helicopter rotor blade, although some attention has been focused on the choice of an appropriate turbulence model[24] for this class of problems.

4. Conclusions.

Solutions of the full potential equations for the unsteady flow around helicopter rotor blades have matured rapidly in recent years to a point where there is little scope for further significant improvement. The full potential equations have been applied successfully to the flow on the advancing side of the rotor disc and are able to predict with reasonable accuracy all of the inviscid flow phenomena described in Section (2).

Methods based upon the Euler equations have become common in the last ten years and have been applied to the flow around advancing rotor blades with reasonable accuracy. Comparison with state of the art potential solvers is disappointing with very little significant improvement being obtained for a substantial increase in computational expense (the only real advantage of using the Euler equations instead of the full potential equation is to capture strong shocks. Strong shocks are however not commonly found in rotorcraft flowfields). For this reason it is unlikely that the solution of the Euler equations will receive much attention in future work, except as a stepping stone to the solution of the full Navier-Stokes equations.

In recent years solutions of the unsteady, compressible Navier-Stokes equations have begun to appear for the flowfield around rotors in hover and forward flight. At the present time the use of such methods has been restricted to the advancing rotor. Significant improvements have been obtained over inviscid methods for transonic flow conditions.

The application of the Navier-Stokes equations to the retreating side of the rotor disc is likely to be the next significant step forward in the modelling of rotor flows. No such work has currently been published although some work has been done to evaluate the performance of turbulence models for such flows. While solutions for

the retreating blade may be possible provided that the flow remains attached, or lightly stalled, there is concern over the ability of current turbulence models to simulate transition between laminar and turbulent flow and massively separated flows which are of great importance if dynamic stall is to be addressed.

Acknowledgements.

This work is supported by the Engineering and Physical Science Research Council (EPSRC).

References.

1. Caradonna, F.X. — **The application of CFD to rotary wing flow problems.** Nasa TM-102803. March 1992.

2. Bezard, H. — **Rotor blade aerofoil design by numerical optimisation and unsteady calculations.** 48th Annual forum of the American Helicopter Society, Washington D.C. June 1986.

3. Srinivasan, G.R. Baeder, J.D. — **TURNS: A freewake Euler/Navier-Stokes numerical method for helicopter rotors.** AIAA Journal Volume 31, Number 5. May 1993.

4. Rai, M. — **Navier-Stokes simulations of Blade Vortex Interaction using high order accurate upwind schemes.** AIAA-87-0543. January 1987.

5. Carr, L. — **Progress in the analysis and prediction of dynamic stall.** Journal of Aircraft Volume 25, Number 1. January 1988.

6. Walker, J.M. Helin, H.E. Strickland, J.H. — **An experimental investigation of an airfoil undergoing large amplitude pitching moments.** AIAA Journal Volume 23, Number 8. August 1985.

7. Yang, H.Q. — **Numerical simulation of dynamic stall at high Reynolds numbers.** AIAA-94-0286. 1994.

8. Caradonna, F.X. Tung, C. — **A review of current finite difference rotor flow methods.** 42nd Annual forum of the American Helicopter Society, Washington D.C. June 1986.

9. Caradonna, F.X. — **Application of transonic flow analysis to helicopter rotor problems.** In Unsteady transonic Aerodynamics edited by D. Nixon. 1989.

10. Sankar, L.N. Tung, C. — **Euler calculations for rotor configurations in unsteady forward flight.** 42nd Annual Forum of the American Helicopter society, Washington D.C. June 2-4 1986.

11. Lock, R.C. Williams, B.R. — **Viscous-Inviscid interactions in external aerodynamics.** Progress in Aerospace Sciences Volume 24 Number 2. 1987

12. Polz, G. (et al) **Current European research activities on the development of advanced CFD methods for the design of rotor blades.** Proceedings of the 17th European Rotorcraft forum, 24-27 September 1991 Berlin, Germany.

13. Perry, F.J. **Aerodynamics of the helicopter world speed record.** 43rd Annual Forum of the American Helicopter society, St. Louis, Missouri. May 1987.

14. Rajagopalan, R.G. Mathur, S.R. **Three dimensional analysis of a rotor in forward flight.** Journal of the American Helicopter Society, Volume 38, number 4. July 1993.

15. Lock, R.C. **A modification to the method of Garabedian and Korn.** In Numerical methods for the computation of inviscid transonic flows with shock waves.

16. Deese, J.E. Argarwal, R.K. **Euler calculations for the flowfield of a helicopter rotor in hover.** Journal of Aircraft, Volume 24 Number 4 April 1987.

17. Deese, J.E. Argarwal, R.K. **An Euler solver for calculating the flowfield of a helicopter rotor in hover and forward flight.** AIAA Paper 87/1427 January 1987.

18. Sankar, L.N. Smith, M.J. **Evaluation of a fourth order compact operator scheme for Euler/Navier-Stokes simulations of rotors in hover.**

19. Chang, I. Tung, C. **Euler solution of the transonic flow for a helicopter rotor.** AIAA Paper 87/0523 January 1987.

20. Chang, I. **Transonic flow analysis for rotors Part 3 - Three dimensional quasi-steady Euler calculation.** Nasa TP 2375, June 1990.

21. Ekaterinaris, J. A. **Effects of spatial order of accuracy on the computation of vortical flow fields.** Technical Note. AIAA Journal, Volume 32, Number 12 December 1994.

22. Holst, T. L. et al. **Viscous Transonic Airfoil Workshop Compendium of results.** AIAA Paper 87/1460 June 1987.

23. Yang, H. **Numerical simulation of dynamic stall at high Reynolds numbers.** AIAA Paper 94/0286 1994.

24. Ekaterinaris, J. A.
Menter, F.R.
Computation of oscillating airfoil flows with one- and two-equation turbulence models. AIAA Journal, Volume 32, Number 12. December 1994.

25. Srinivasan, G.R.
Ekaterinaris, J.A.
McCroskey, W.J.
Dynamic stall of an oscillating wing. Part 1: Evaluation of turbulence models.
AIAA Paper 93/3403 1993.

26. Scott, M. T.
Narramore, J.C.
Navier-Stokes correlation of swept helicopter rotor tips at high alpha. AIAA CP 91/1752 1991.

27. Wake, B.E.
Solution procedures for the Navier-Stokes equations applied to rotors. PhD Dissertation Georgia Institute of Technology, April 1987.

28. Wake, B.E.
Sankar, L.N.
Solutions of the Navier-Stokes equations for the flow about a rotor blade. Journal of the American Helicopter Society, Volume 34, Number 2. April 1994.

29. Srinivasan, G.R.
McCroskey, W.J.
Navier-Stokes calculations of hovering rotor flowfields. Journal of Aircraft, Volume 25, Number 10.

30. Caradonna, F.X.
Tung, C.
Experimental and analytical studies of a model helicopter in hover. Vertica, Volume 5, pages 149-161. 1981.

31. Srinivasan, G.R.
Baeder, J.D.
TURNS: A freewake Euler/Navier-Stokes numerical method for helicopter rotors. Technical Note, AIAA Journal, Volume 31, Number 5. 1993.

32. Srinivasan, G.R.
Baeder, J.D.
Flowfield of a lifting rotor in hover. A Navier-Stokes simulation. AIAA Journal, Volume 30, Number 10. October 1992.

33. Srinivasan, G.R.
Raghavan, V.
Duque, E.P.N.
McCroskey, W.J.
Flowfield analysis of modern helicopter rotors in hover by Navier-Stokes method. Journal of the American Helicopter Society, July 1993.

34. Rajagopalan, R.G.
Mathur, S. R.
Three dimensional analysis of a rotor in forward flight. Journal of the American Helicopter Society, July 1993.

35. Berezin, C.R.
Sankar, L.N.
An improved Navier-Stokes/Full potential coupled analysis for rotors. AIAA Paper 94/0736, 1994.

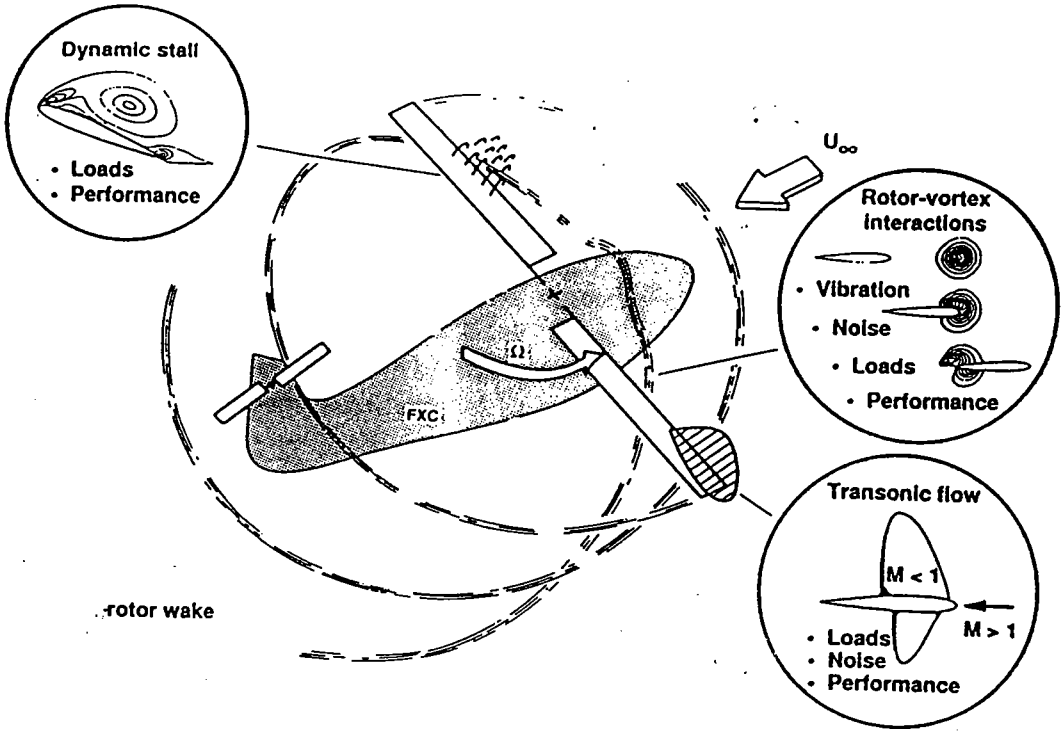

Figure (1). Rotorcraft flow problems.

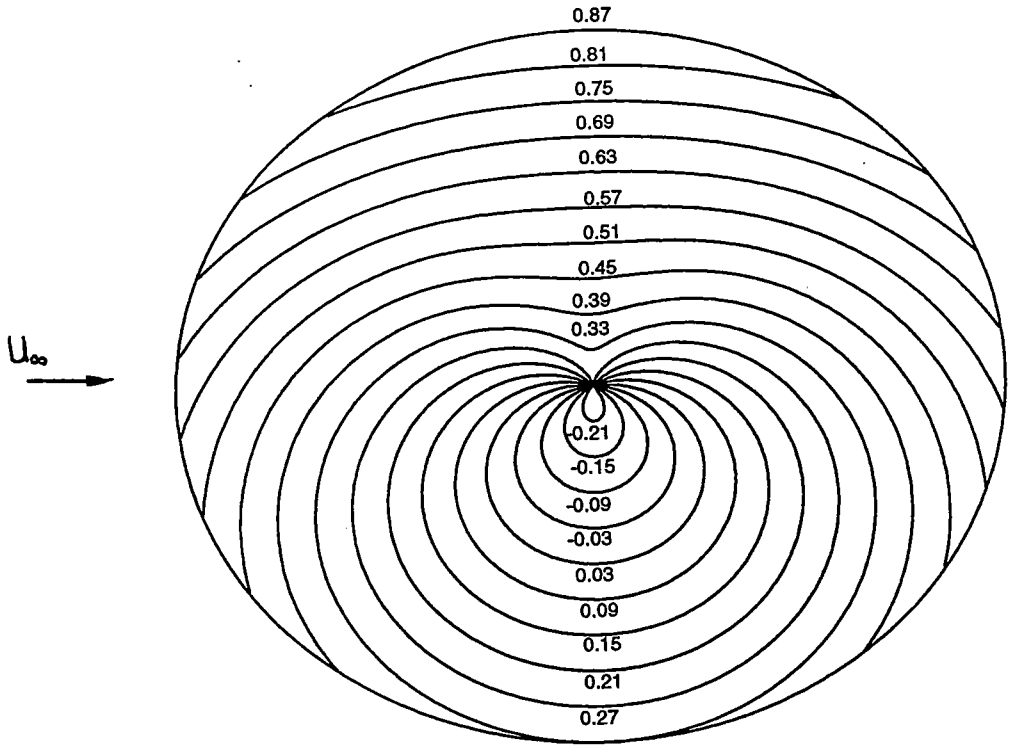

Figure (2) . Freestream Mach number distribution.

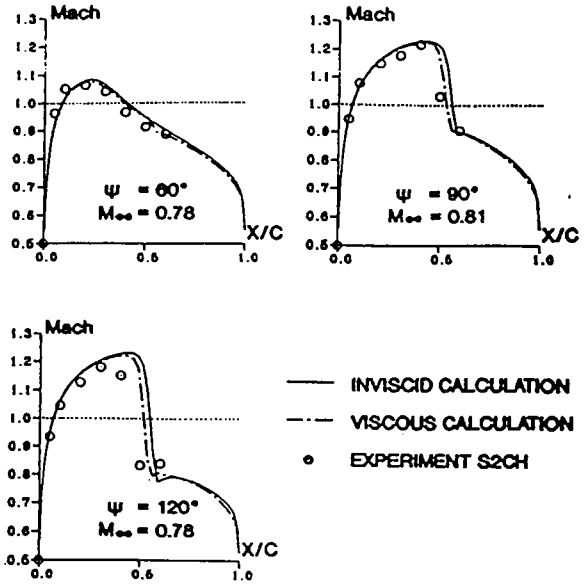

Figure (3). Calculated and experimental unsteady Mach number distributions.

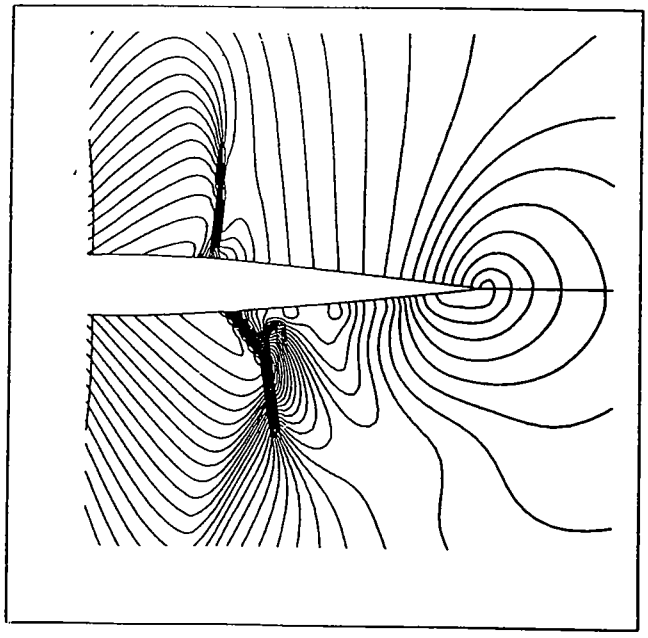

Figure (4). Pressure contours showing shock bifurcation caused by BVI.

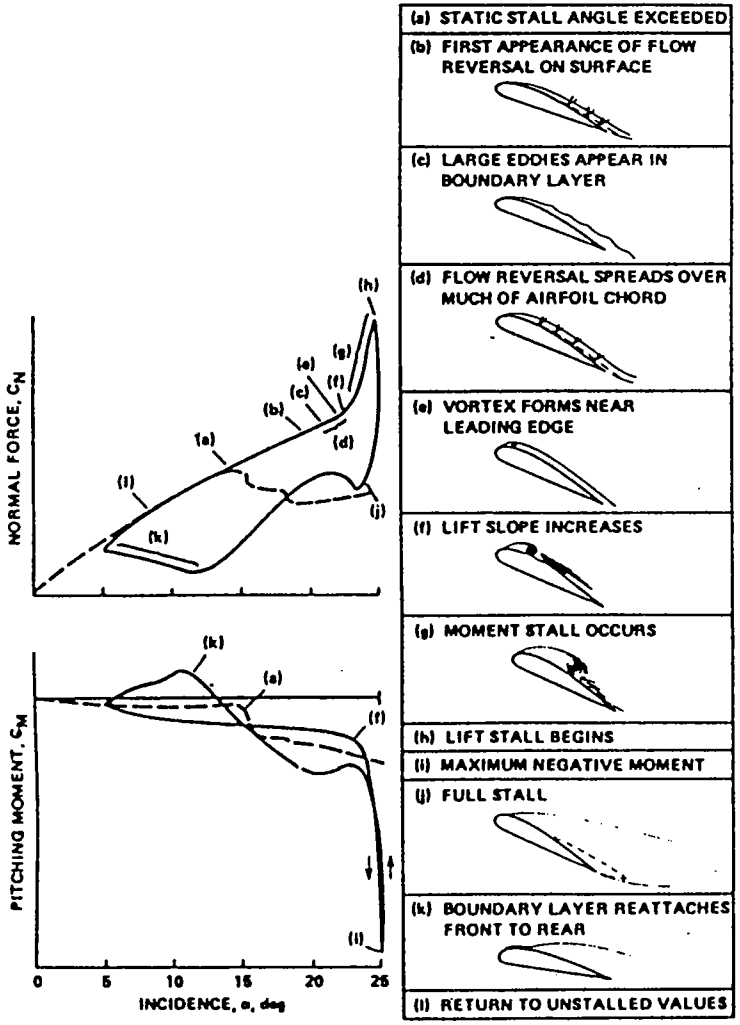

Figure (5). Events of dynamic stall.

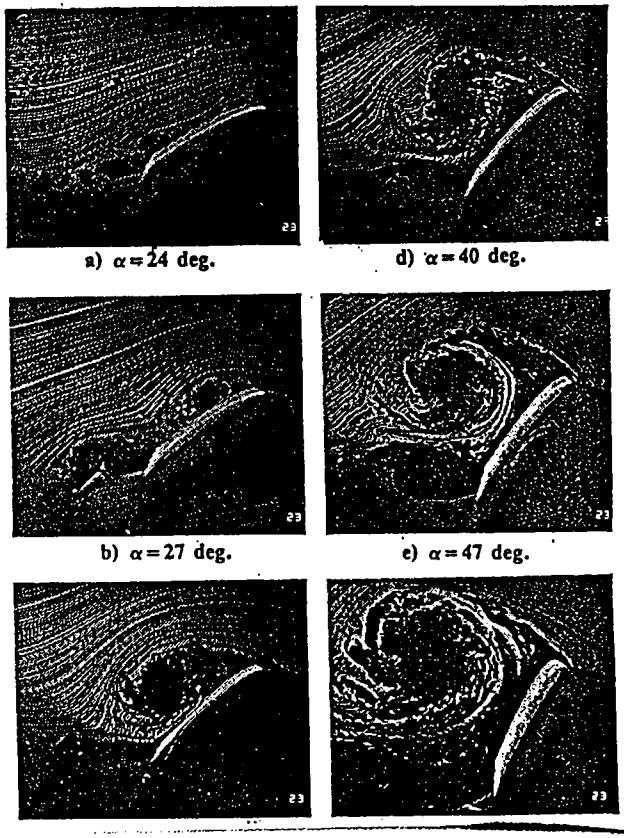

Figure (6). Flow visualisation of dynamic stall.

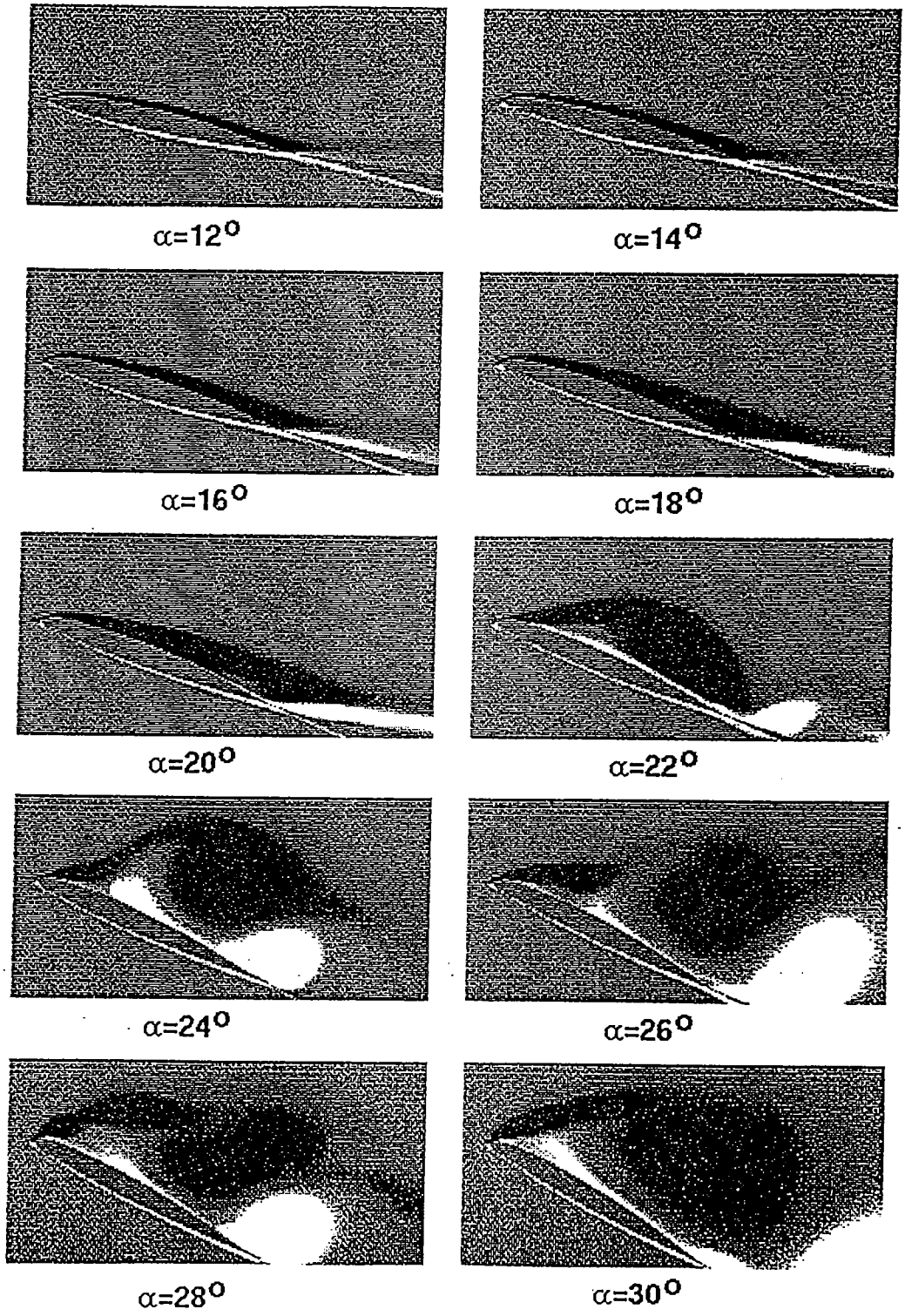

Figure (7). Computational flow visualisation of dynamic stall.

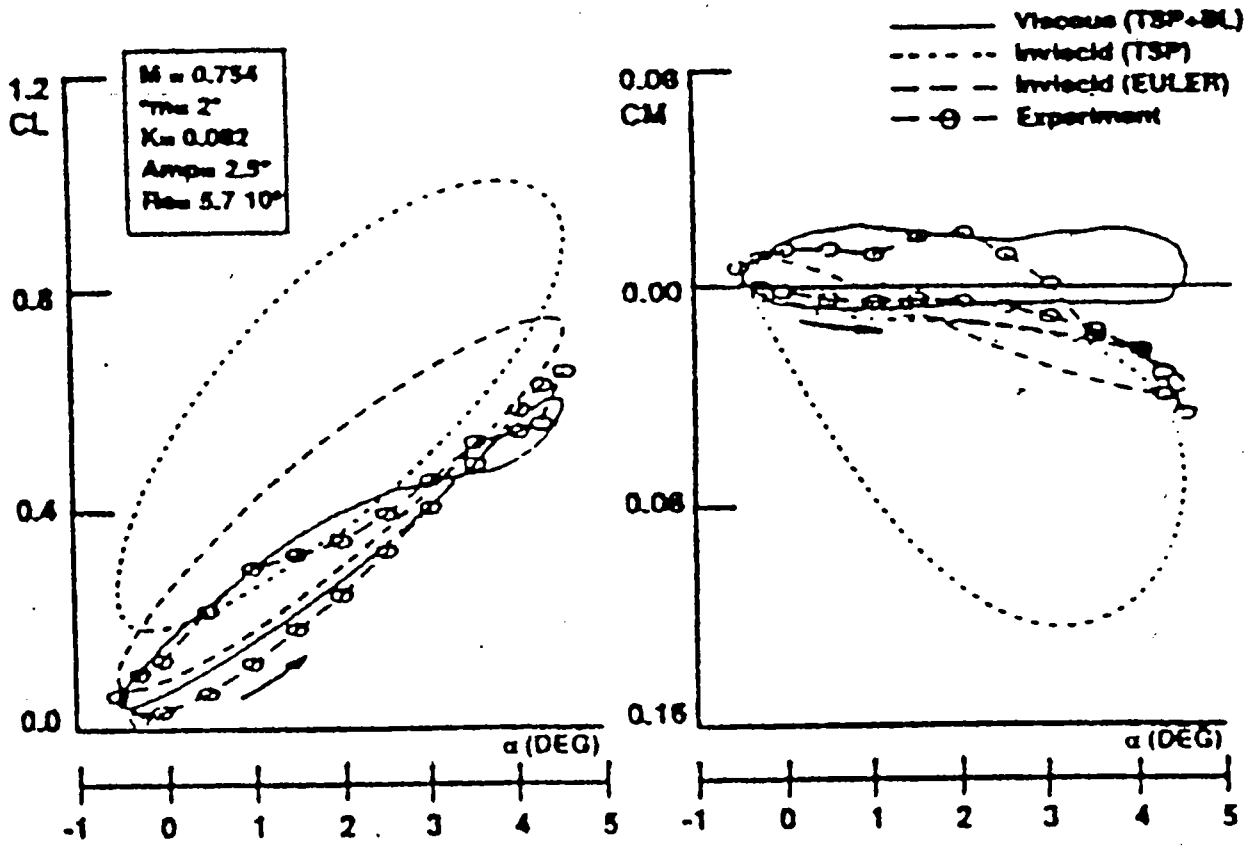

Figure (9). Comparison of full potential codes with experiment (both with and without boundary layer modelling).

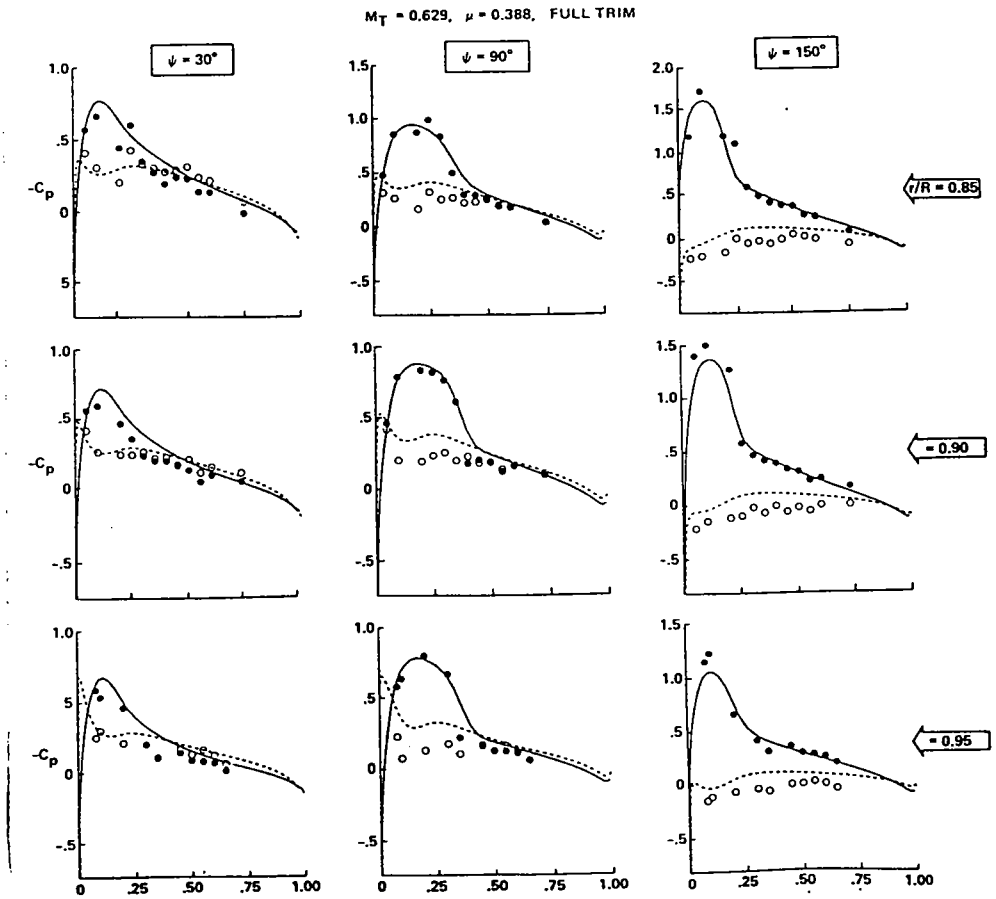

Figure (10). Comparison of full potential method with experiment.

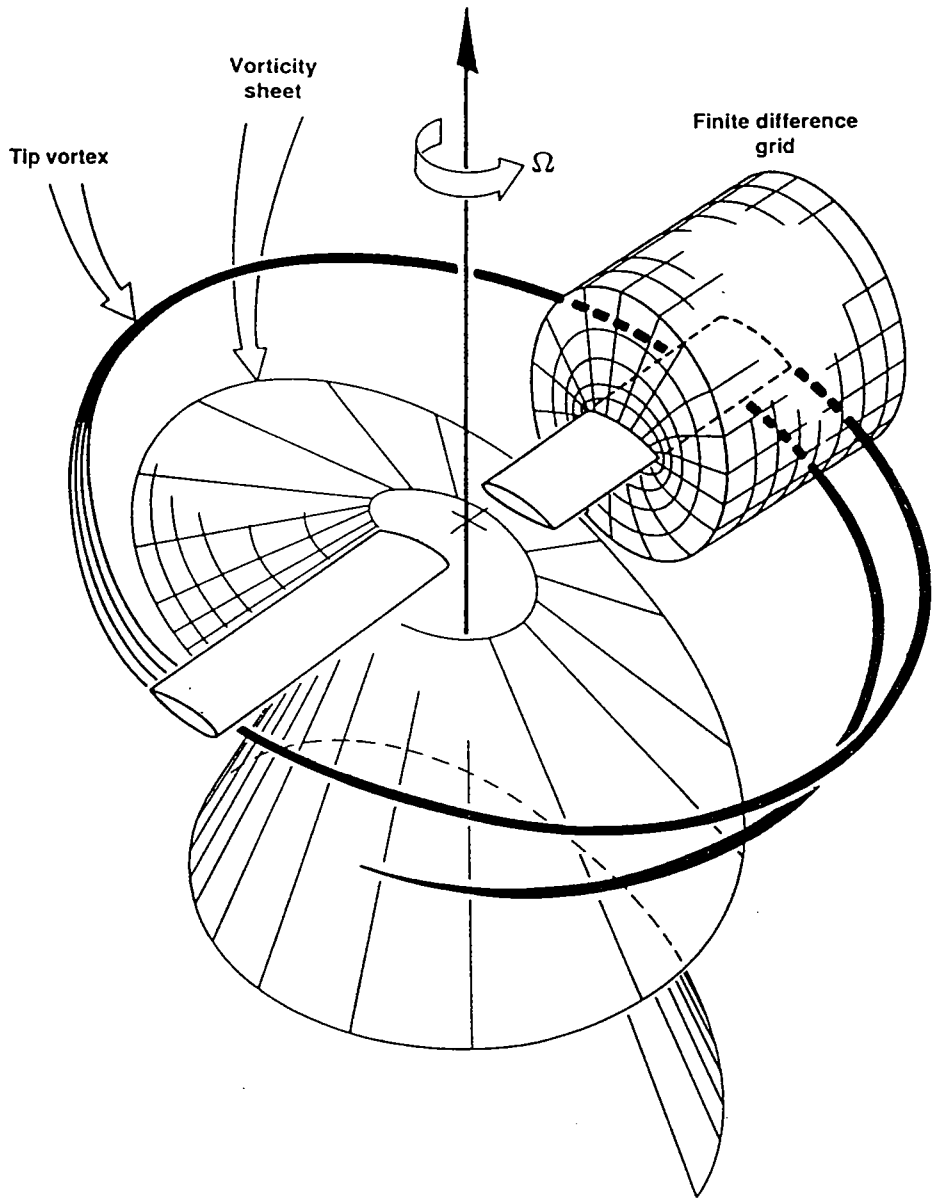

Figure (11). Finite difference grid in global hover flow.

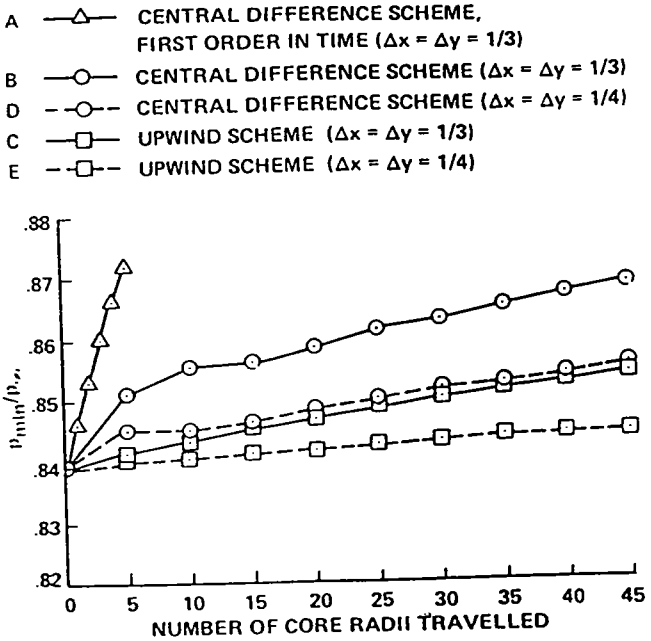

Figure (12). Vortex decay rates for various schemes.

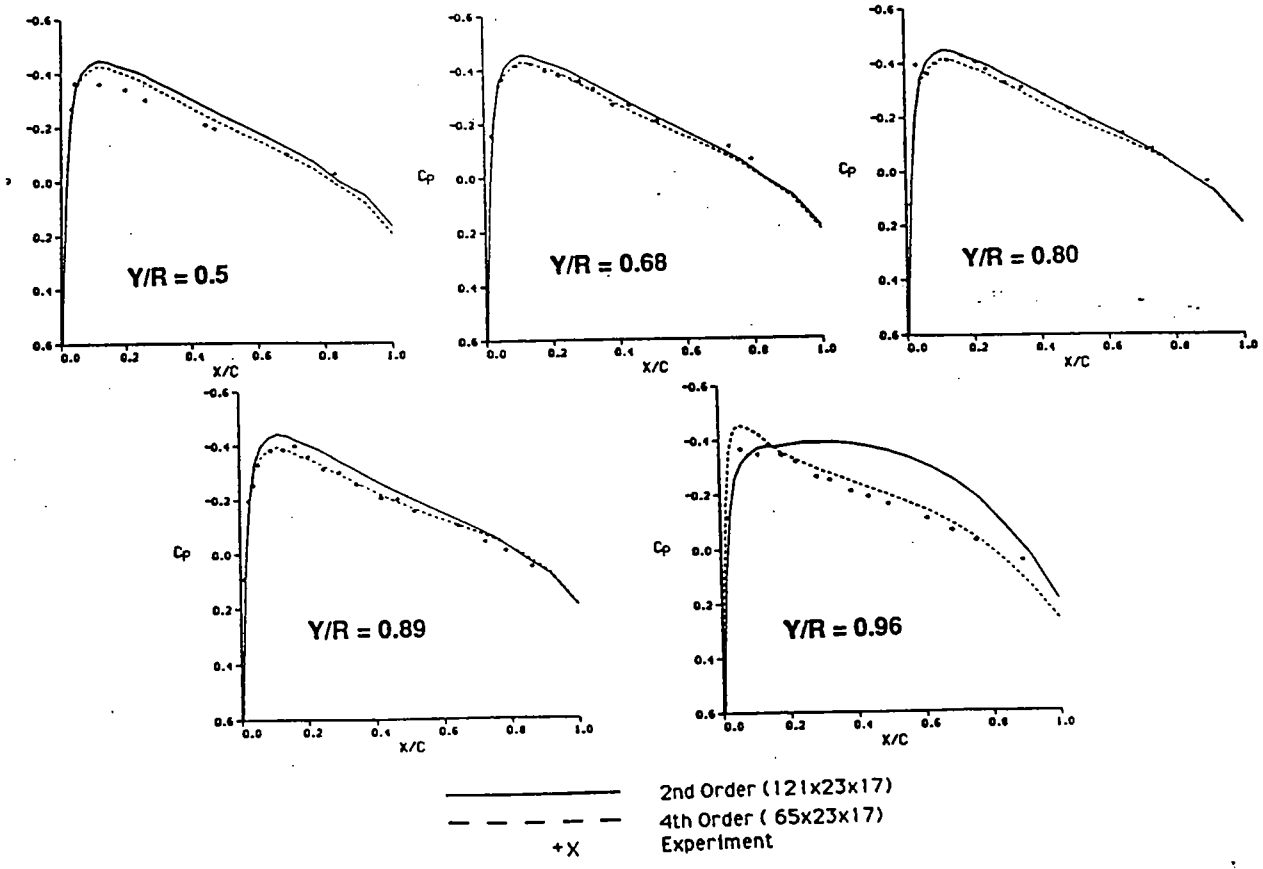

Figure (13). Comparison of second and fourth order Euler schemes.

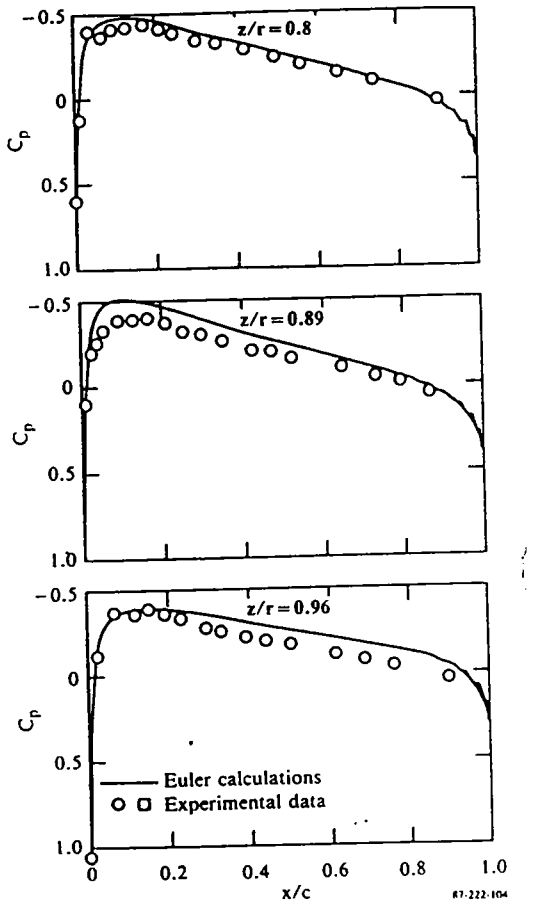

(a) Non-lifting rotor in hover.

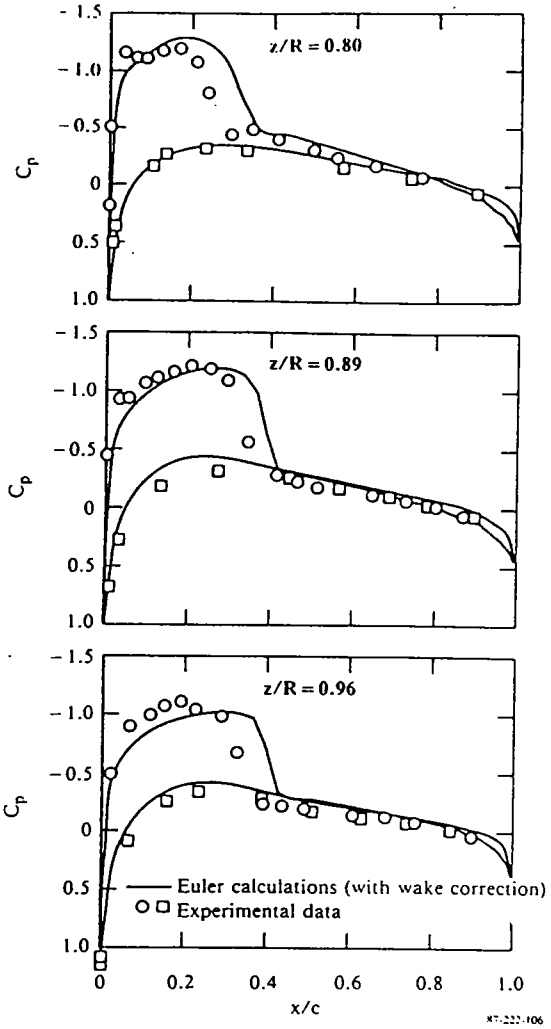

(b) Lifting rotor in hover.

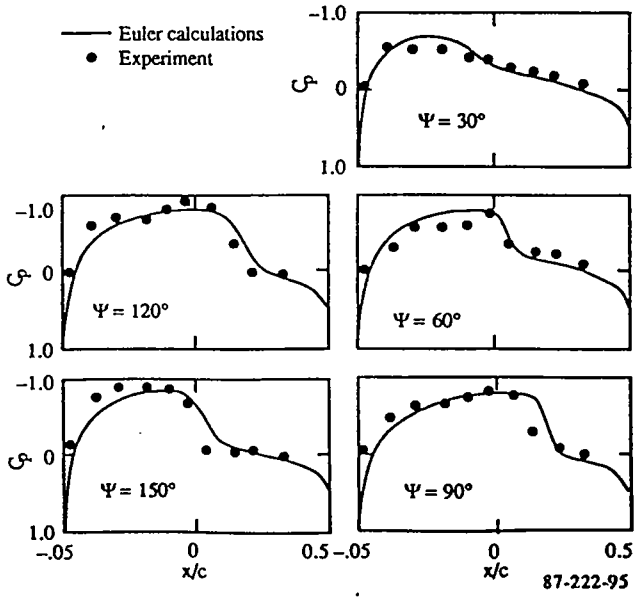

(c) Lifting rotor in forward flight.

Figure (14). Comparison of Euler code with experiment.

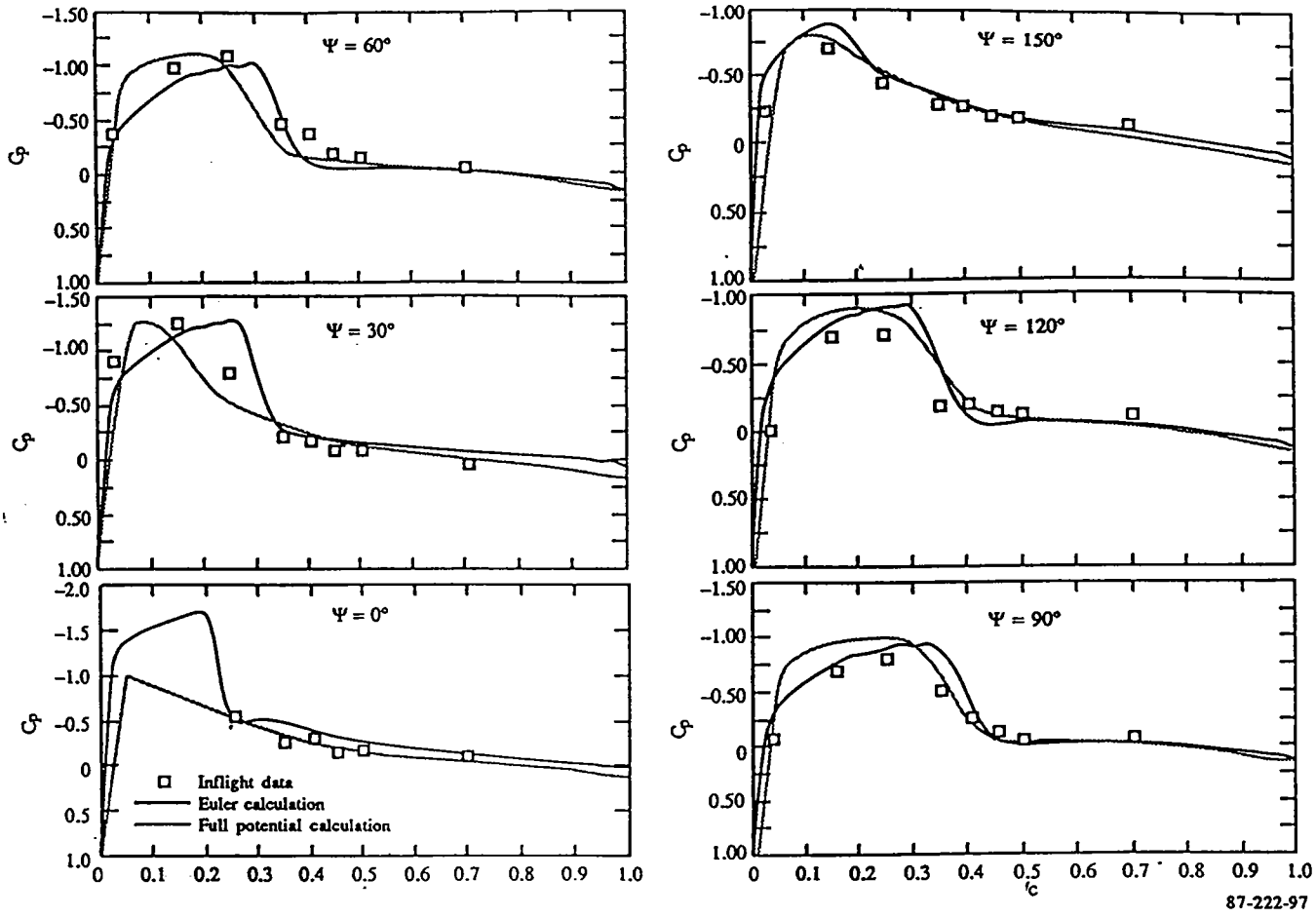

Figure (15). Comparison of Euler and full potential methods with experiment.

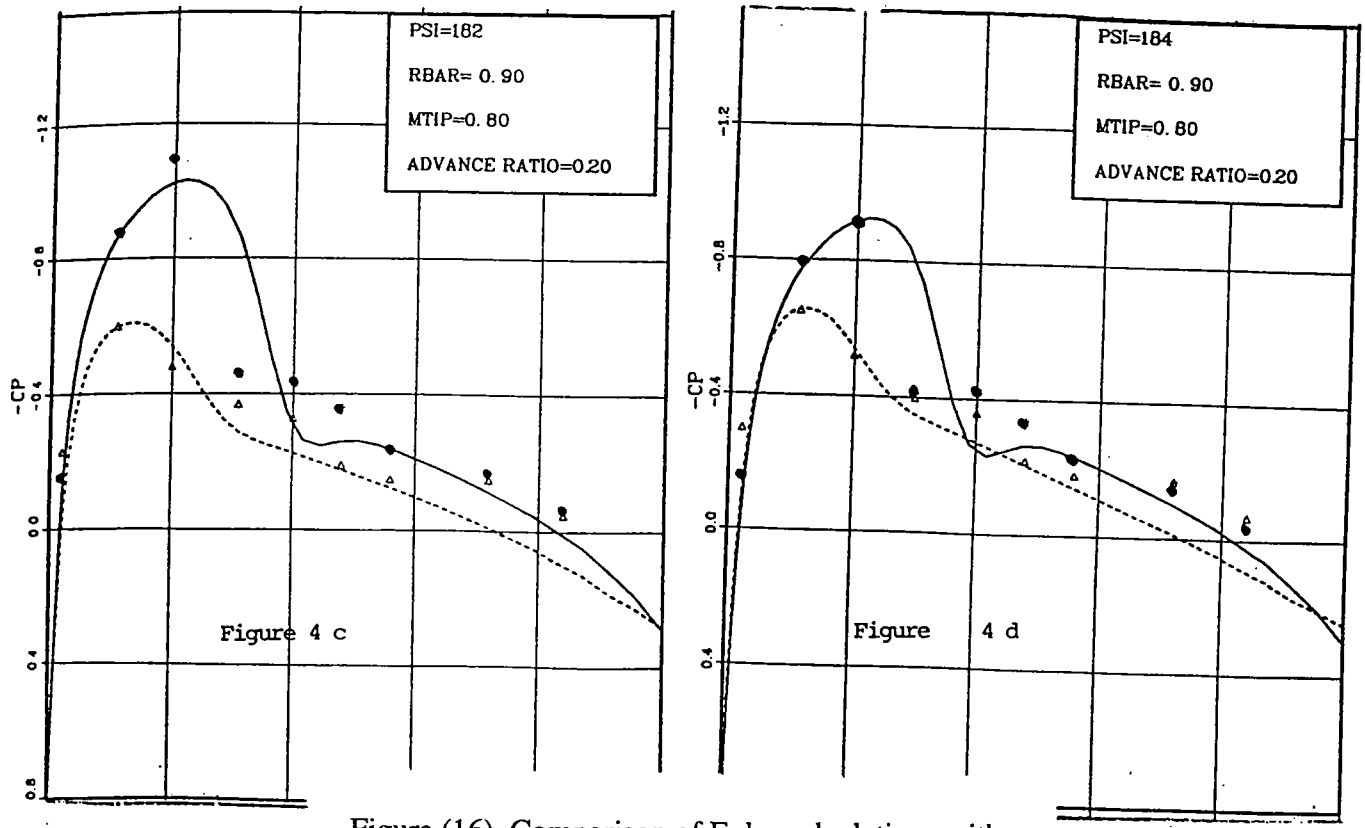

Figure (16). Comparison of Euler calculations with experiment (non-lifting and lifting rotors repectively).

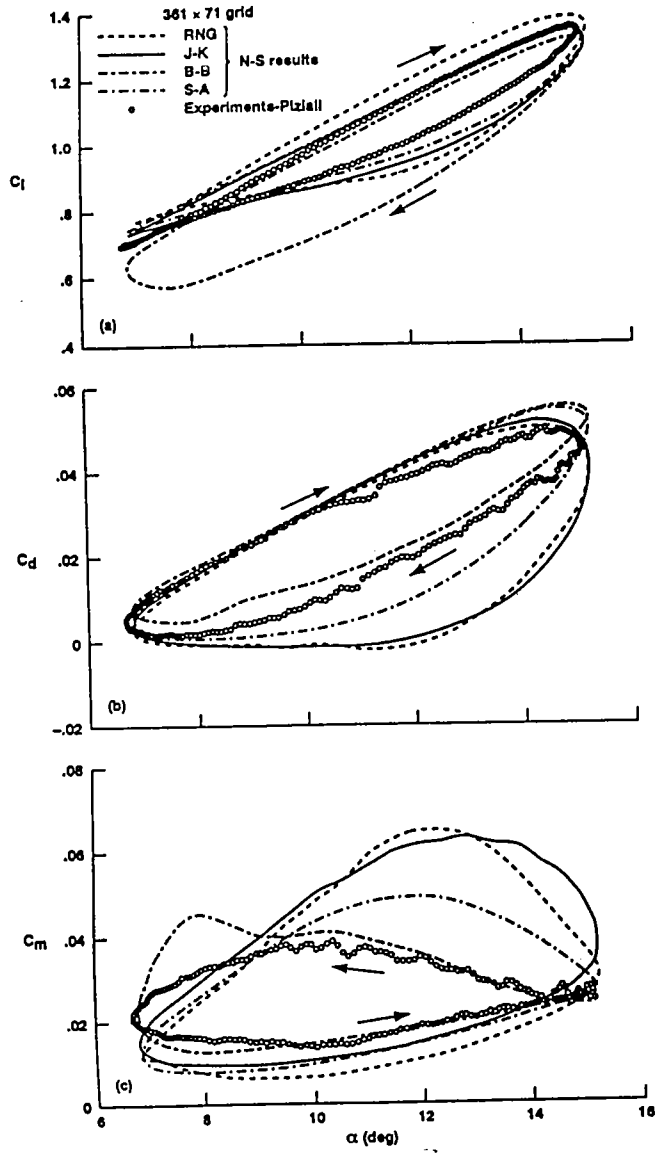

Figure (21). Comparison of unsteady calculated airloads for different turbulence models with experiment (lightly stalled).

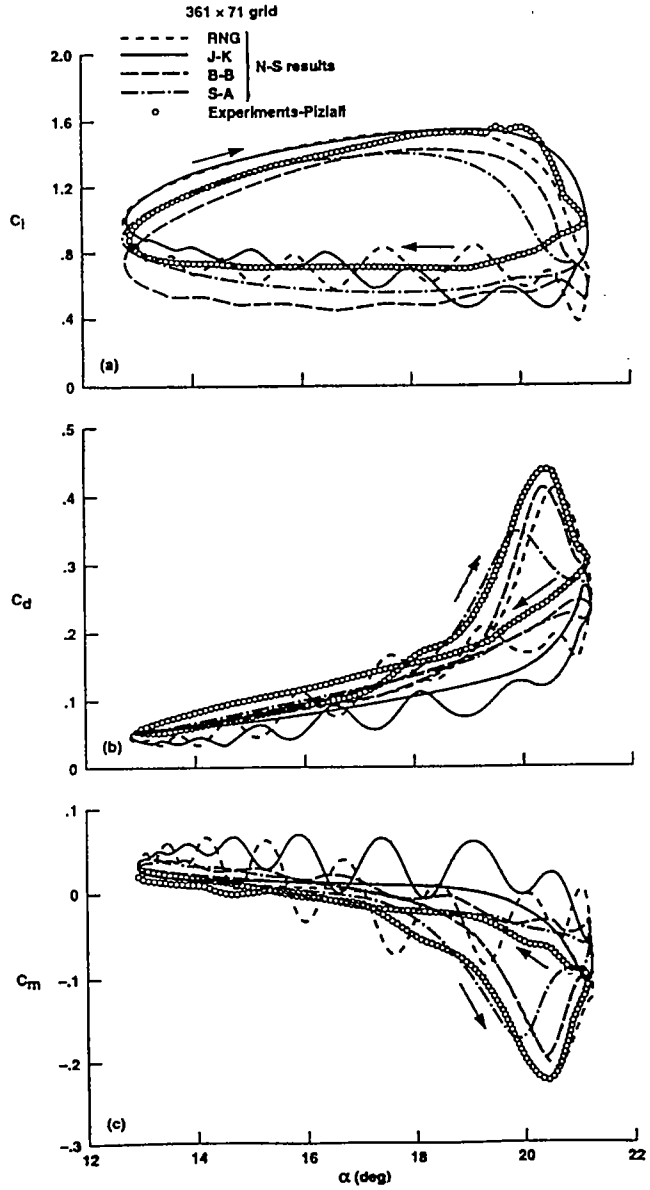

Figure (22). Comparison of unsteady calculated airloads for different turbulence models with experiment (deeply stalled).

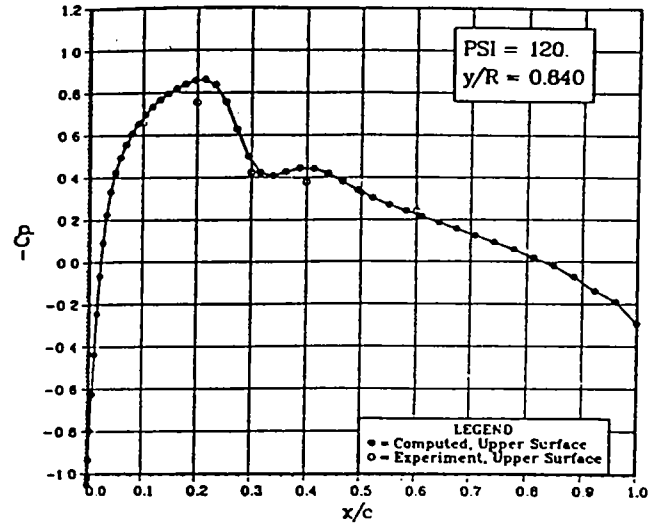

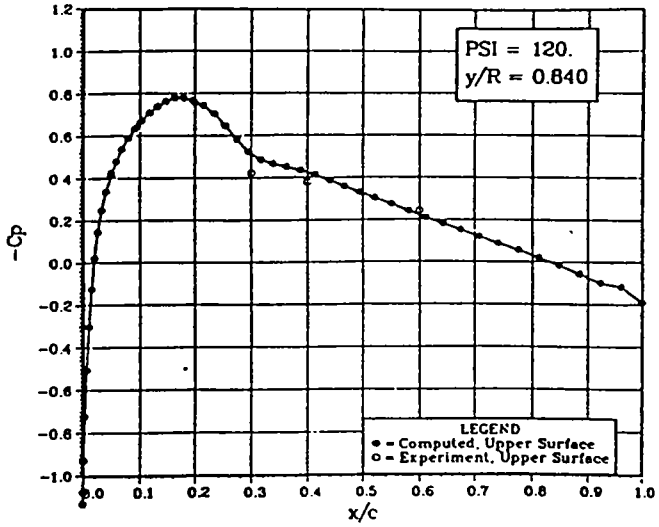

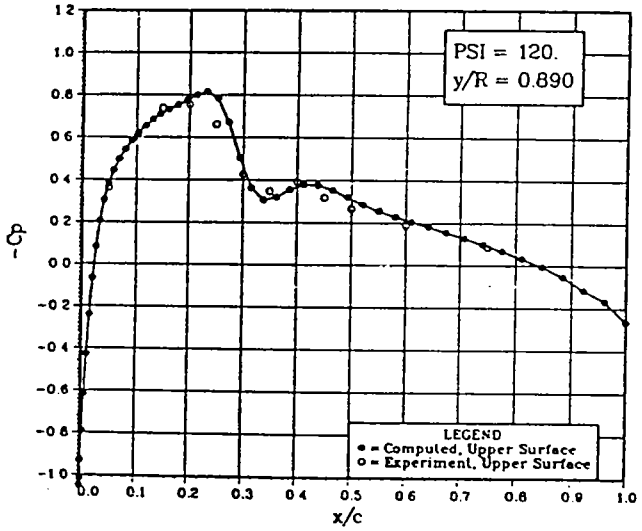

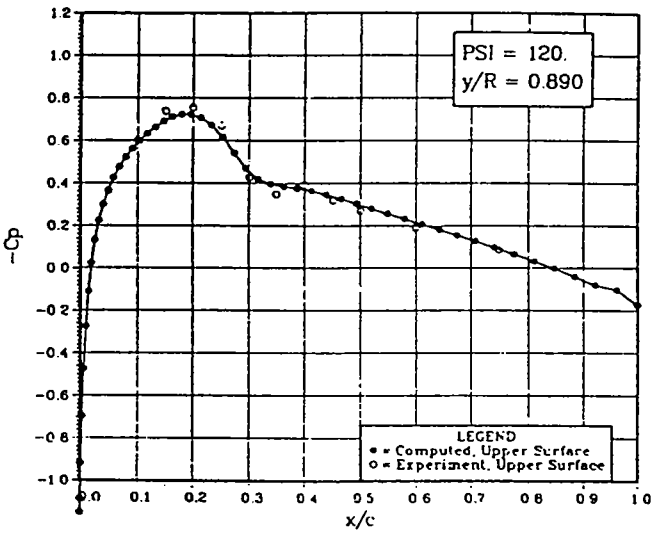

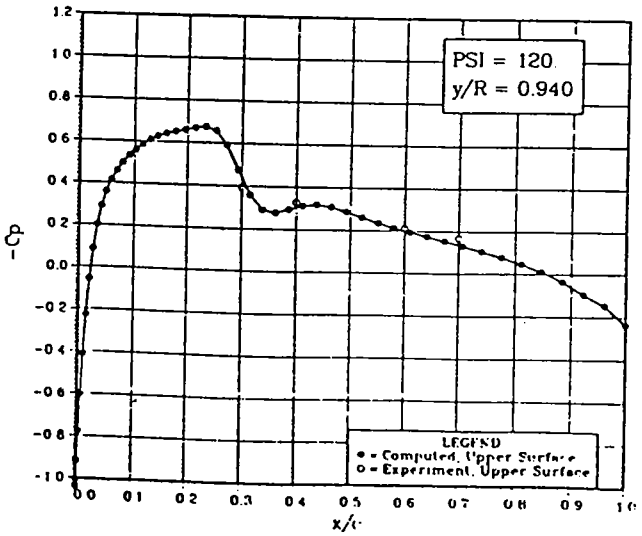

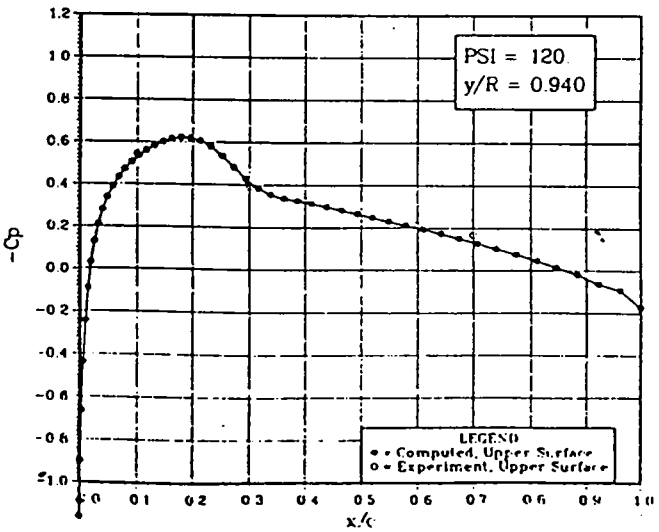

(a) Euler.

(b) Navier-Stokes.

Figure (23). Comparison of Euler and Navier-Stokes codes with experiment.

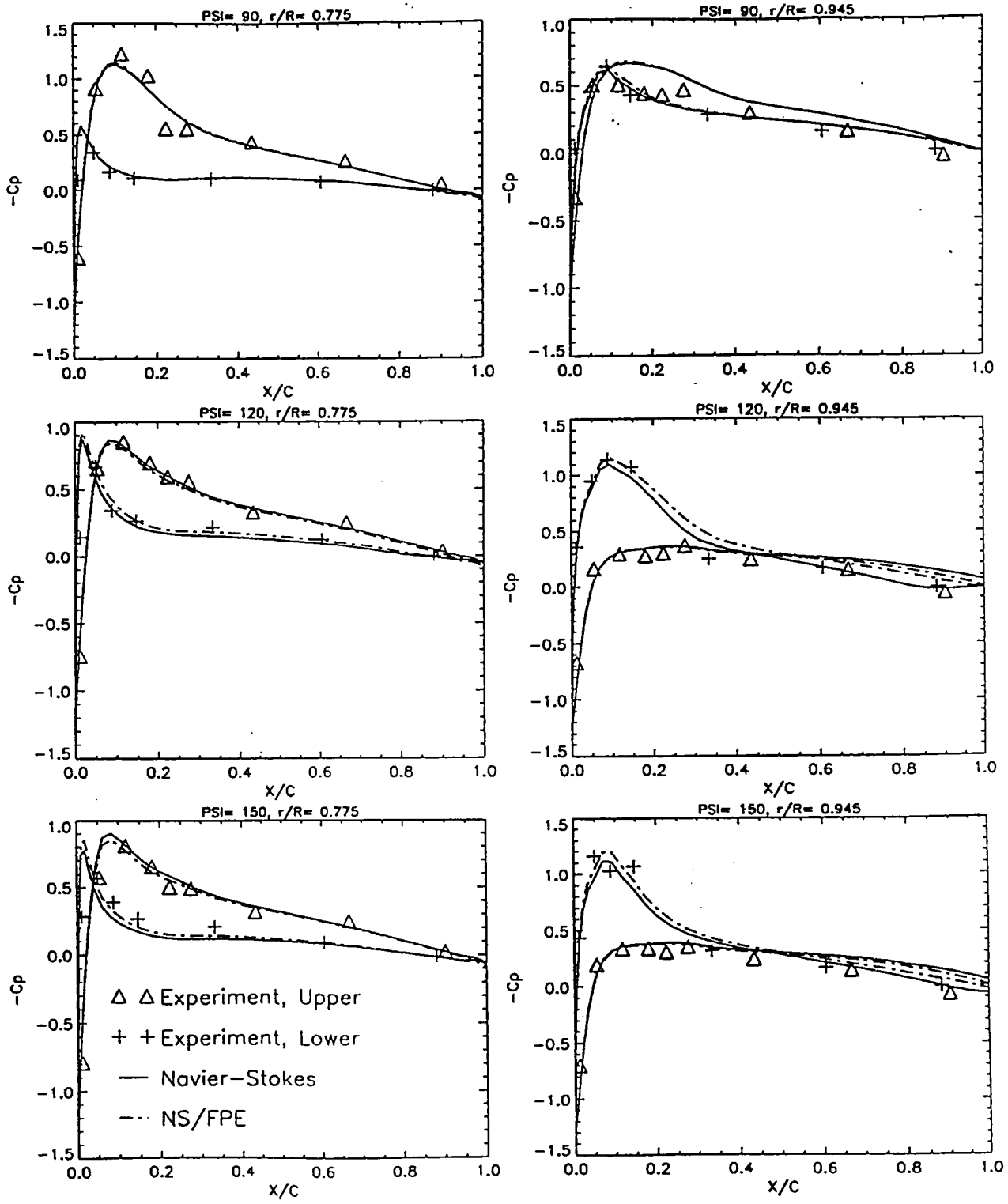

Figure (28). Comparison of coupled method with Navier-Stokes method.

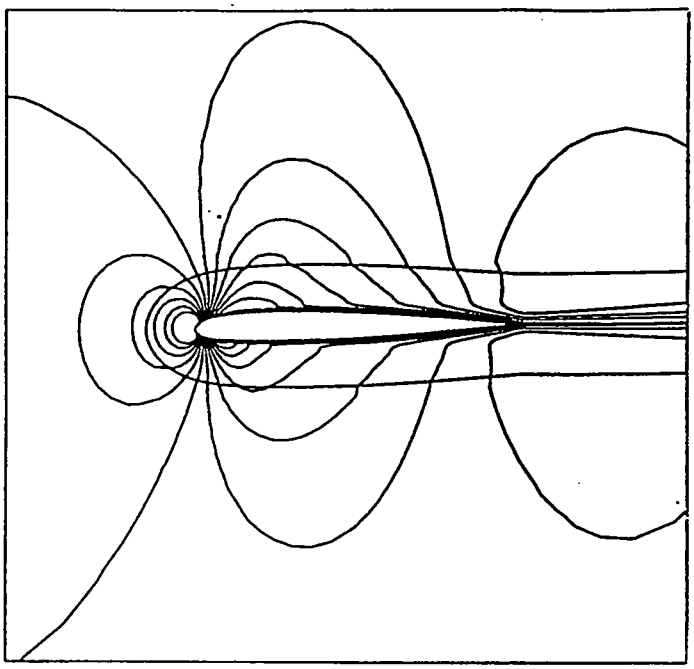

Navier-Stokes/full-potential

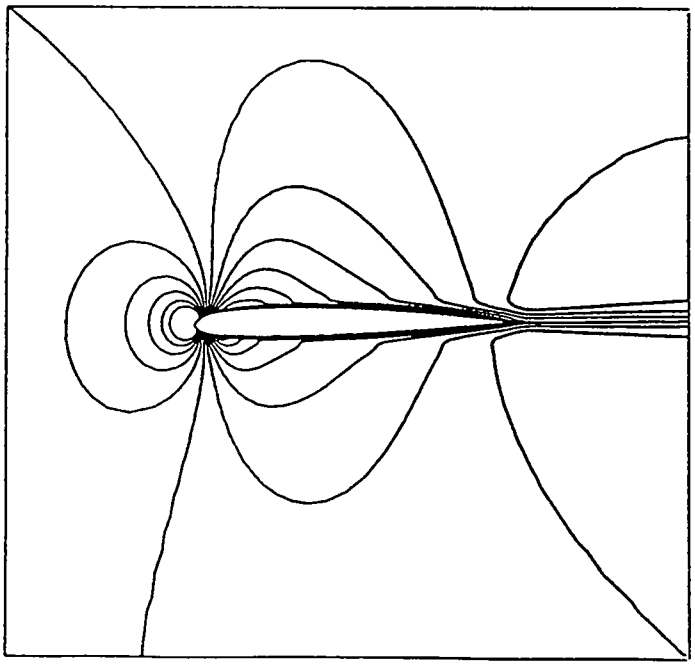

Navier-Stokes

Figure (29). Comparison of coupled method with Navier-Stokes method.